ADVANCED HEALTHCARE MATERIALS
www.advhealthmat.de

# Bone Scaffolds Based on Degradable Vaterite/PEG-Composite Microgels

*Elena Stengelin, Alena Kuzmina, Guillermo L. Beltramo, Martha F. Koziol, Laura Besch, Romina Schröder, Ronald E. Unger, Wolfgang Tremel, and Sebastian Seiffert**

**Vaterite, a metastable modification of calcium carbonate, embedded in a flexible microgel packaging with adjustable mechanical properties, functionality, and biocompatibility, provides a powerful scaffolding for bone tissue regeneration, as it is easily convertible to bone-like hydroxyapatite (HA). In this study, the synthesis and physical analysis of a packaging material to encapsulate vaterite particles and osteoblast cells into monodisperse, sub-millimeter-sized microgels, is described whereby a systematic approach is used to tailor the microgel properties. The size and shape of the microgels is controlled via droplet-based microfluidics. Key requirements for the polymer system, such as absence of cytotoxicity as well as biocompatibility and biodegradability, are accomplished with functionalized poly(ethylene glycol) (PEG), which reacts in a cytocompatible thiol–ene Michael addition. On a mesoscopic level, the microgel stiffness and gelation times are adjusted to obtain high cellular viabilities. The co-encapsulation of living cells provides i) an in vitro platform for the study of cellular metabolic processes which can be applied to bone formation and ii) an in vitro foundation for novel tissue-regenerative therapies. Finally, the degradability of the microgels at physiological conditions caused by hydrolysis-sensitive ester groups in the polymer network is examined.**

## 1. Introduction

Bone injuries have become an increasing health problem due to increasing life expectancy of the population.[1,2] In the United States, for example, more than 6 million fractures and 500 000 bone grafts occur every year, and worldwide, there are more than 20 million patients affected by bone-tissue loss due to trauma and degenerative diseases.[1,3] The skeleton is a central component for body stability, force distribution, and protection of organs, and bone lesions are accompanied by pain and physical limitations. This is accompanied by a loss of personal life quality and considerable costs for the health system and society.[1,4]

Patients with osteoporosis are at particularly high risk for fractures and poorly healing bone injuries.[5] This metabolic disease causes a low bone mineral density and structural bone loss due to an imbalance in the bone remodeling process.[5] Conventional osteoporosis therapies with drugs, such as bisphosphonates, estrogen agonists/antagonists, or teriparatide, primarily aim at inhibiting bone resorption or promoting bone formation, but they do not enable restoration of vanished bone mass.[5,6] Therefore, despite good availability of antiresorptive and anabolic medications, bone fractures are common in patients with osteoporosis and are often the cause of the problems described above.[6] As a result, there is an increasing need for novel therapeutic approaches that promote bone regeneration within a reasonable period of time.[1,6]

A promising regenerative approach might consist of a restorative therapy using a combination of scaffold-based biomaterials and bioactive agents, into which endogenous cells can migrate to build new bone material.[1,7] In addition to ceramics, polymers of synthetic and natural origin are the most popular scaffolding matrix for tissue regeneration, as they allow the 3D structure and biochemical properties of tissue to be mimicked.[1,8] Moreover, they enable the integration of additional bone-regenerating components to obtain mechanically stable and biocompatible composites. Accordingly, Shi et al. developed artificial polymer-HA framework structures to promote bone growth, based on the premise that HA ($Ca_{10}(PO_4)_6(OH)_2$) is the most prevalent component in inorganic bone.[9] However, natural, non-stoichiometric HA is composed of a multitude of ions such as $Mg^{2+}$, $Na^+$, and $CO_3^{2-}$, and depending on the specific bone location and function, there is a wide spectrum of bone mineral variants with regard to structure, composition, and biological behavior.[1,10] As a result, synthetically

E. Stengelin, A. Kuzmina, M. F. Koziol, L. Besch, Dr. R. Schröder, Prof. W. Tremel, Prof. S. Seiffert
Johannes Gutenberg University Mainz
Department of Chemistry
Mainz D-55128, Germany
E-mail: sebastian.seiffert@uni-mainz.de
Dr. G. L. Beltramo
Institute of Biological Information Processing 2 (IBI-2)
Jülich Forschungszentrum GmbH
Jülich D-52428, Germany
Dr. R. E. Unger
Johannes Gutenberg University Mainz
Institute of Pathology
Mainz D-55128, Germany
The ORCID identification number(s) for the author(s) of this article can be found under https://doi.org/10.1002/adhm.201901820



**DOI: 10.1002/adhm.201901820**

produced stoichiometric HA has only a limited capability of reaching the versatility of its natural counterpart.[11]

To overcome such limitations, an alternative approach is to provide a suitable form of a calcium precursor to support bone mineralization in situ. Vaterite, which is a metastable modification of calcium carbonate, is such a promising calcium precursor, as it is easily convertible to bone-like hydroxycarbonate apatite (HCA).[10,12,13] When provided in the form of micrometer-sized particles, it is highly biocompatible with human osteoblasts and endothelial cells, and hence, it may represent a suitable platform for rapid in situ bone regeneration.[10,12,13] Vaterite in combination with endogenous cells and in a flexible packaging form with adjustable mechanical properties, functionality, and biocompatibility might be a powerful starting point for tissue regeneration.[14,15]

To accomplish this, certain conditions must be met. Any preclinical development of a biotherapeutic material is generally characterized by a sequence of in vitro and in vivo optimization cycles, where the in vivo phase is complex, time consuming, and expensive. In contrast, the preceding in vitro phase is generally less time consuming and expensive. Thus, the introduction of living cells to the in vitro phase would allow for a rational, early-stage optimization of the biocompatibility of all materials and the entire therapeutic process. This, in turn, would reduce the time and cost for the subsequent in vivo phase. Moreover, exposing composite bone-promoting matrix materials to bone-derived living cells would also allow for a detailed study of bone formation processes in vitro.

A suitable method to combine vaterite particles and living cells homogeneously in a flexible packing form is droplet-based microfluidic technology. This method enables the synthesis of monodisperse and uniform micrometer-sized hydrogels with exquisite control over their geometry. It also enables the controlled micro- and nanoencapsulation of further additives such as cells and drugs.[16]

To provide a basis for such rational materials engineering, this paper aims to i) introduce a convenient in vitro platform for the study of metabolic processes in bone formation and ii) provide an in vitro foundation for novel tissue-regenerative therapies. We report on the development of system where a model matrix composed of osteoblast cells and vaterite particles are co-embedded within 3D hydrogel-based structures designed and produced by droplet-based microfluidics (**Figure 1**). Our approach includes the development of monodisperse, sub-millimeter-sized hydrogel scaffolds, directed by a systematic parameter control. On a macroscopic level, microfluidic droplet templating enables the production of size- and shape-defined specimens with the option of controlled cell and vaterite encapsulation. On a microscopic level, key requirements for the polymer system, such as the absence of cytotoxicity as well as good biocompatibility and biodegradability, are achieved by the use of functionalized PEG.[14,17] Harmful radicals and toxic catalysts are avoided by the use of bio-orthogonal and cytocompatible thiol–ene Michael addition chemistry to induce droplet gelation.[18] On a mesoscopic level, the microgel properties, such as their mechanical stiffness and gelation time, are adjusted to obtain high cellular viabilities by control of the polymer concentration, precursor polymer size, and the reaction conditions during gelation. Based on this systematic approach, physicochemically tailored scaffolding structures with bone matrix-specific properties are designed to eventually degrade under physiological conditions.

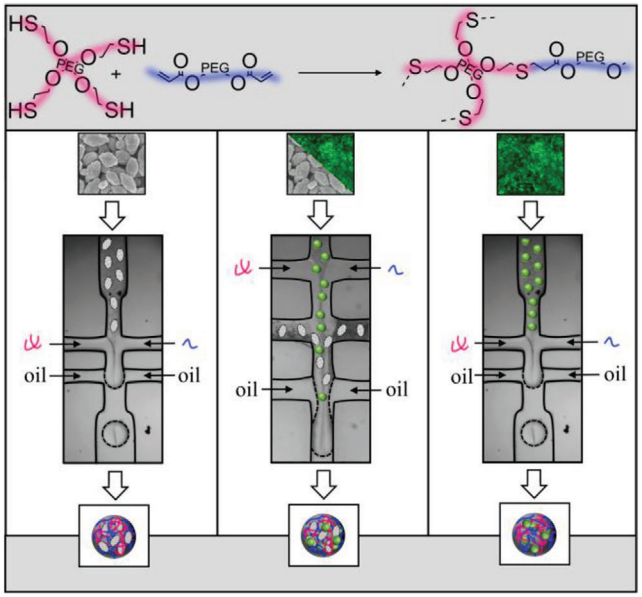


**Figure 1.** Production scheme for the encapsulation of vaterite particles (left), osteoblast cells (right), as well as a combination of both (middle) in a uniform sub-millimeter-sized microgel package formed by droplet-based microfluidics. Gelation of the precursor polymers is carried out by a biocompatible Michael addition between PEG-based thiol- and acrylate-functionalized precursor polymers.

## 2. Results and Discussion

### 2.1. Polymer Scaffold

#### *2.1.1. Basis*

Biocompatible PEG is chosen as the starting material for generating microgels containing living cells and vaterite particles since it is FDA approved and commercially available in a variety of pre-functionalized forms, architectures, molar masses, and narrow distribution of the latter. As a result, this polymer provides a suitable model platform in which key parameters for tailored hydrogel generation can be controlled and explored. Based on this material, the production of polymer-network gels is performed by using PEG building blocks with star-shaped and linear topologies. Thiol-functionalization of the star-shaped precursors (4-arm PEG-thiol) and acrylate-functionalization of the linear precursors (linear PEG-acrylate) allows the precursors to be linked by radical-free and biocompatible Michael addition (see reaction scheme in Figure 1). Since the Michael addition reaction generally takes place in alkaline medium, the precursor polymers are dissolved in a slightly alkaline, biocompatible phosphate buffer at pH 7.2. Due to subsequent experiments involving living cells, the precursor polymers are also dissolved in Dulbecco's Modified Eagle Medium (DMEM) as a culture medium for cells with a pH at physiological conditions (37 °C and 5% $CO_2$) of 7.2–7.4.

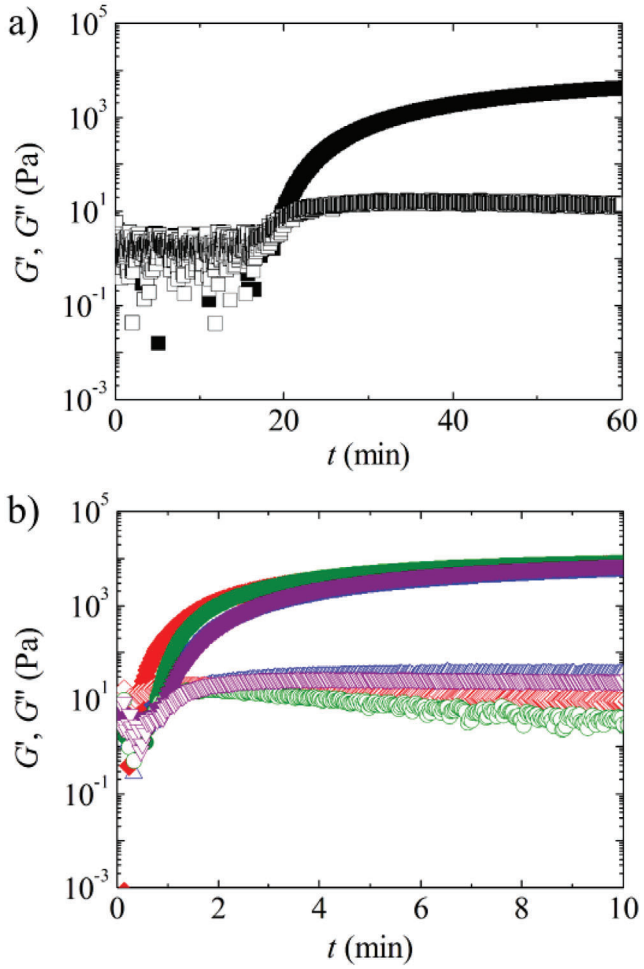


**Figure 2.** Time-dependent rheology measurements of the [4-arm PEG-thiol 10 000 g mol$^{-1}$ (10K)/linear PEG-acrylate 5000 g mol$^{-1}$ (5K)] composition with a mean mass concentration of 160 g L$^{-1}$ in a) phosphate buffer and b) in cellular medium DMEM. Herein, the crossing point of storage modulus, $G'$, and loss modulus $G''$ indicates gelation. (a) In phosphate buffer ($G'$ (■), $G''$ (□)), gelation occurs after approximately 20 min, (b) whereas it occurs in less than a minute in DMEM ($G'$ (▼), $G''$ (▽)). Additional time-dependent rheology measurements of the same precursor polymers under cross-linking conditions in DMEM with several supplements (1% Gl [$G'$ (●), $G''$ (○)], 1% Gl + 10% FBS [$G'$ (◆), $G''$ (◇)], 1% Gl + 10% FBS + 1% P/S [$G'$ (▲), $G''$ (△)]) show no influence of these on the gelling time; they all exhibit an increase of the complex viscosity within about 1 min.

For comparative analyses of the precursor-polymer solution gelation time in phosphate buffer and in DMEM, time-dependent rheology measurements are performed. For this purpose, a [4-arm PEG-thiol 10 000 g mol$^{-1}$ (10K)/linear PEG-acrylate 5000 g mol$^{-1}$ (5K)] composition with a mean mass concentration of 160 g L$^{-1}$ is used. The evolution of the storage modulus, $G'$, and the loss modulus $G''$ is monitored as a function of time $t$, as shown in **Figure 2**a. In these experiments, the crossing point of $G'$ and $G''$ indicates gelation. In phosphate buffer ($G'$ (■), $G''$ (□)), gelation occurs after approximately 20 min at room temperature. By contrast, gelation occurs after less than 1 min in DMEM ($G'$ (▼), $G''$ (▽)) at room temperature (Figure2b). The reasons for the fast gelling in DMEM are probably additional ingredients as salts and amino acids in the cell culture medium and also the slightly higher pH value of the medium as compared to that of the phosphate buffer: since the Michael addition preferably occurs in alkaline solutions, an increased basicity leads to an increased reaction rate.

In addition, the influence of additives to the medium, such as GlutaMAX (Gl), fetal bovine serum (FBS), and penicillin/streptomycin (P/S), on the reaction rate is studied by time-dependent rheology. The resulting curves ($G'$ and $G''$ as a function of time $t$), are shown in Figure 2b. Gelation in DMEM (1% Gl) ($G'$ (●), $G''$ (○)) as well as DMEM (1% Gl, 10% FBS) ($G'$ (◆), $G''$ (◇)) and DMEM (1% Gl, 10% FBS, 1% P/S) ($G'$ (▲), $G''$ (△)) leads to crossing of $G'$ and $G''$ within 1 min and is therefore similar to the reaction in pure DMEM ($G'$ (▼), $G''$ (▽)). Major influences of these additives on the gelling time are therefore considered to be negligible.

Due to the use of thiol-functionalized building blocks, oxidative disulfides can be formed in a competing side reaction to the Michael addition. To estimate the rate of this side reaction, time-dependent rheology measurements of the 4-arm PEG-thiol 10K precursor (mass concentration of 160 gL$^{-1}$) dissolved in physiological phosphate buffer as well as in DMEM (1% Gl, 10% FBS, 1% P/S) are performed in the absence of the Michael-reactive linear PEG-acrylate precursor. Again, the crossing point of $G'$ and $G''$ indicates gelation. It appears that the disulfide formation and the subsequent gelation in cell culture medium DMEM (1% Gl, 10% FBS, 1% P/S) occurs within a few hours. The reasons for the fast gelling in DMEM are probably a high oxygen level in the solution as well as a high amount of nutrients and salts in the medium. Furthermore, 4-arm PEG-thiol 10K precursor linkages to thiol-containing components in the culture medium DMEM, such as amino acids (e.g., cysteine) and proteins, have to be considered as well. In comparison, we observe a longer gelation in phosphate buffer. Depending on the batch of the polymers, the gelation time varies between approximately 10 to 48 h. Since disulfides are formed faster in the cell culture medium DMEM (1% Gl, 10% FBS, 1% P/S) than in phosphate buffer, further microfluidic experiments are done using phosphate buffer as the solvent, or a mixture of both.

### 2.1.2. Droplet-Based Microfluidics

Droplet-based microfluidic devices are used to form microgel particles from the heterofunctional PEG precursors. These devices can also be simultaneously used to embed cells and vaterite particles as bone-regeneration supporting supplements into the microgels. We employ two different poly(dimethylsiloxane) (PDMS) devices fabricated by soft lithography, that are shown schematically in Figure 1. The devices displayed on the left and on the right side are designed for the preparation of either vaterite- or cell-containing microgels, whereas the device shown in the middle of the scheme is designed for the simultaneous preparation of vaterite- and cell-containing microgels (for details, see Figures S1 and S2, Supporting Information).

The microfluidic device for the encapsulation of either vaterite particles or cells exhibits a rectangular cross-section of 100 µm

diameter, intersecting at two sequential cross-junctions. At the first junction, aqueous solutions or suspensions of the two precursor polymers (4-arm PEG-thiol and linear PEG-acrylate), cells, or vaterite particles combine to form a laminar co-flowing stream. At the second junction, addition of an immiscible carrier fluid (HFE fluorinated oil/PFPE–Tris surfactant) serves to break the stream into monodisperse droplets with a uniform size of 150–200 µm in diameter, depending on the flow rates and the precursor solution viscosities. In these droplets, surrounded by oil, the two polymeric building blocks react in a radical-free, biocompatible thiol–ene Michael addition and form 3D polymer networks within a few minutes.

The microfluidic device designed for the simultaneous encapsulation of vaterite particles and cells is composed of channels that exhibit rectangular cross-sections of 100 µm diameter, intersecting at three sequential cross-junctions. In the first junction, aqueous solutions of the two precursor polymers (4-arm PEG-thiol and linear PEG-acrylate) and the cell suspension are injected and combined. In the second junction, a water miscible vaterite/ethylene glycol suspension is injected. At the third junction, addition of an immiscible carrier fluid (HFE fluorinated oil/PFPE–Tris surfactant) serves to break this fluid stream into monodisperse droplets with a uniform size of 160 µm in diameter.

In a subsequent purification step, the resulting microgel particles synthesized using both microfluidic devices are freed from the oil and transferred to an aqueous environment. Depending on the microgel composition and the aqueous environment (phosphate buffer or DMEM), they swell to uniform sizes in the range of 200–300 µm in these media.

### 2.2. Vaterite-Containing Microgels

#### *2.2.1. Vaterite Synthesis and Analytics*

Vaterite is a meta-stable modification of calcium carbonate and converts to bone-like HCA under physiological conditions.[12,19] In combination with a PEG-based packaging form, this could be a useful compound for in situ bone regeneration.

The synthesis of vaterite particles is carried out by sonification of a mixture of calcium chloride dihydrate and sodium bicarbonate in ethylene glycol until a precursor vaterite solution is obtained.[12,19] The particle size of vaterite in the precursor solution is monitored by dynamic light scattering (DLS), which denotes polydisperse particles in the range of diameters between 200 and 600 nm (for details see Figure S3, Supporting Information). Since vaterite particles are more stable in the dry state than in suspension, they are precipitated from the precursor vaterite/ethylene glycol mixture by addition of water and then dried under high vacuum. The precipitated nanoparticles agglomerate to micrometer-sized clusters, as shown by scanning-electron microscopy imaging (SEM) (**Figure 3**a). The nanoparticles as well as their larger agglomerates have characteristic ellipsoidal morphologies. Further particle characterization is performed by Fourier-transform infrared spectroscopy (FT-IR) and Raman spectroscopy (Figure 3b,c). The resulting spectra show characteristic $CO_3^{2-}$ vibrational frequencies of vaterite and verify its identity (antisymmetric $\nu_3$ stretching mode at 1487–1411 $cm^{-1}$, symmetric $\nu_1$ stretching mode at 1090 $cm^{-1}$, out-of-plane bending motion $\nu_2$ at 877 $cm^{-1}$, and in-plane bending motion $\nu_4$ at 744 $cm^{-1}$).[10,12]

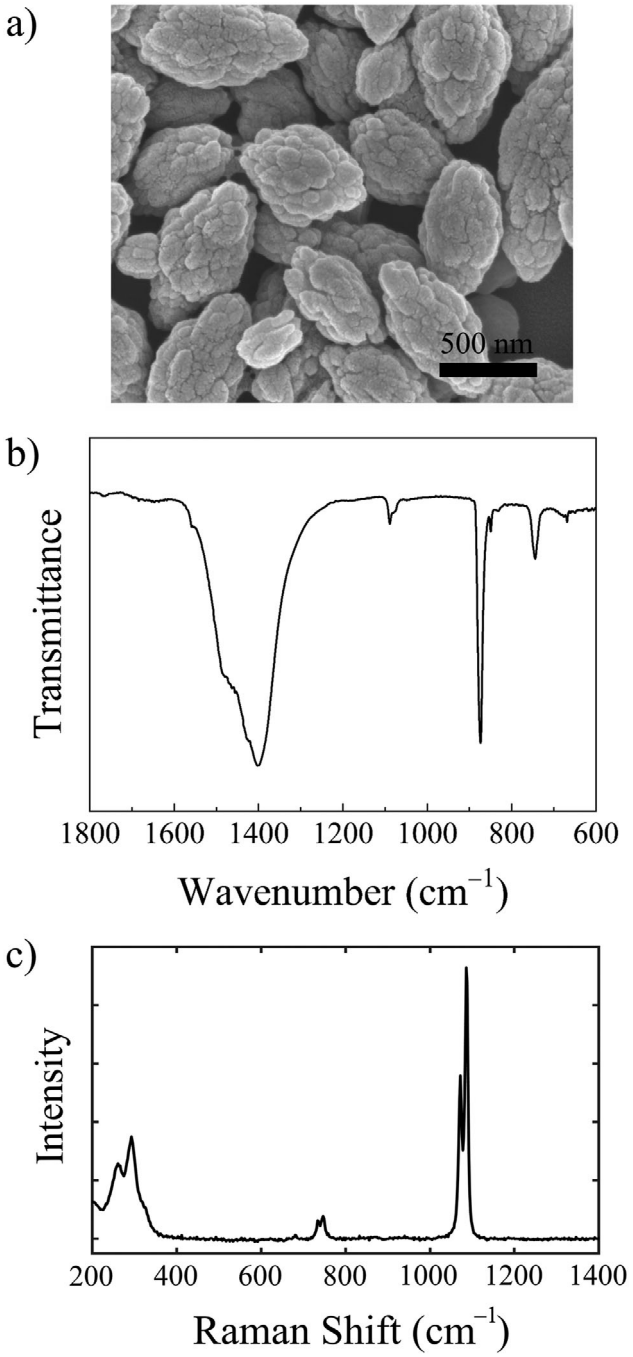


**Figure 3.** Characterization of vaterite particles. a) Scanning electron microscopy (SEM) image of vaterite particles. b) FT-IR and c) Raman spectra show the characteristic $CO_3^{2-}$ vibrational bands of vaterite (1487–1411 $cm^{-1}$: antisymmetric $\nu_3$ stretching mode; 1090 $cm^{-1}$: symmetric $\nu_1$ stretching mode; 877 $cm^{-1}$: out-of-plane bending mode $\nu_2$; 744 $cm^{-1}$: in-plane bending motion $\nu_4$).

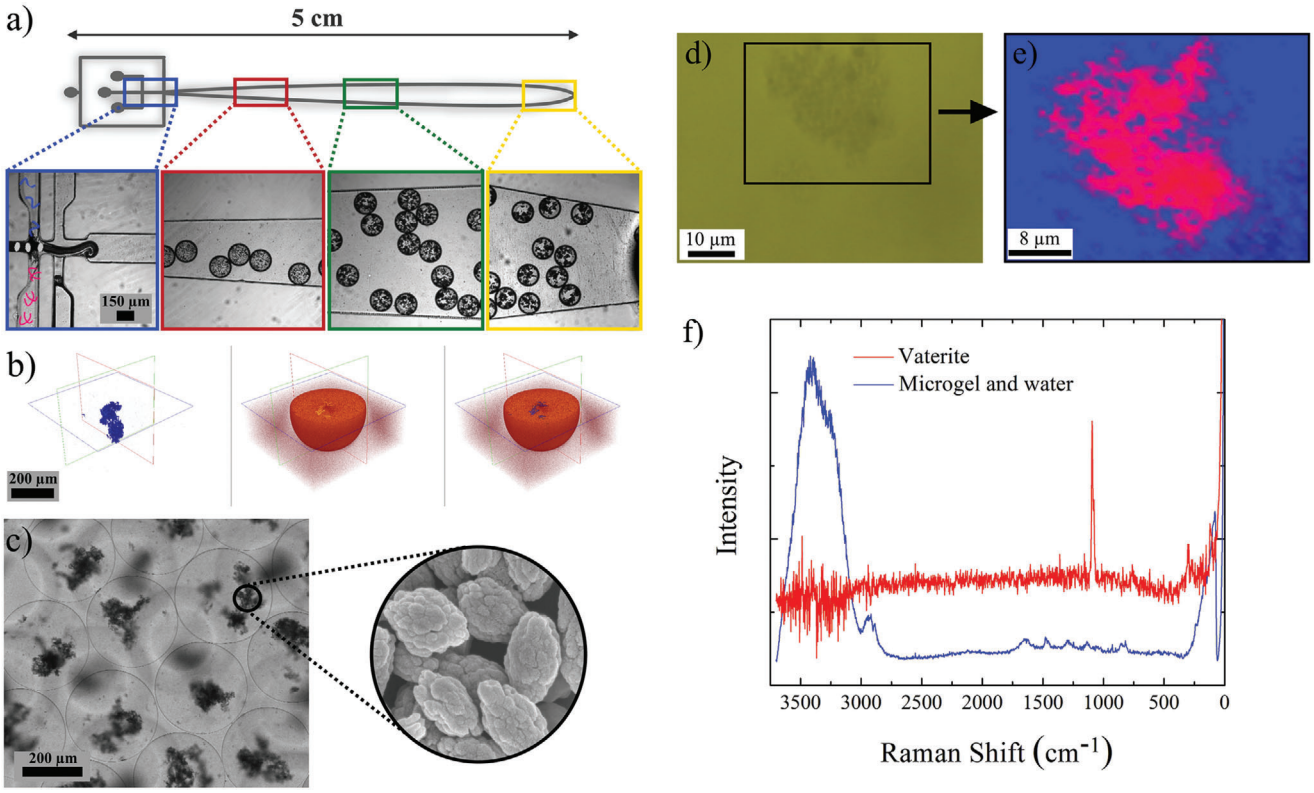


**Figure 4.** Images and analysis of vaterite-containing microgels. a) Schematic representation of the microfluidic device used for this experiment, including four sections (framed in blue, red, green, and yellow, respectively) displaying the droplets at different second-scale dwell times in the channel system. Vaterite particles in the droplets agglomerate increasingly to clusters after encountering the aqueous building block solution in the first cross-section, as is depicted in the sequence of the four sections. b) The resulting vaterite-containing microgels are analyzed by 3D confocal laser scanning microscopy and selective staining with sulforhodamine B and calcium-selective tetracycline, as well as c) by the transmission path of the confocal laser scanning microscope. d) Bright-field image of vaterite particles located in a microgel, whereby a small section of the microgel is depicted. e) Confocal Raman image from the black squared area of the bright-field image. The red area shows the vaterite agglomerates, and the blue area shows the microgel fragment, stored in water. f) Raman spectrum from the vaterite agglomerates (red) and the combined spectrum of the microgel fragment and water (blue). The spectra are obtained by hyperspectral analysis of the confocal Raman image.

### *2.2.2. Encapsulation of Vaterite Particles*

Vaterite particles are encapsulated into microgels using the microfluidic device depicted in **Figure 4**a. The four sections are passed by the droplets at different dwell times in the channel system. The section framed in blue shows the two rectangular cross-sections of the microfluidic device that are overlaid by schematics of the injected linear PEG-acrylate precursors (blue), star-shaped 4-arm PEG-thiols (red), and vaterite particles (gray). The sections framed in red, green, and yellow show the droplets a few seconds after their formation.

Microgel formation occurs after injection of aqueous 4-arm PEG-thiol 10 000 g $mol^{-1}$ (10K) and linear PEG-acrylate 5000 g $mol^{-1}$ (5K) precursor polymer solutions (dissolved in phosphate buffer) with a mean mass concentration of 300 g $L^{-1}$ each at the first junction of the microfluidic device, along with vaterite particles resuspended in ethylene glycol (5% w/v) by ultrasonic mixing. Droplets of the mixture of these components are formed at the second junction by flow-focusing with a non-miscible fluorinated oil. In these droplets, the precursor polymers react in a radical-free, biocompatible Michael addition, while vaterite particles agglomerate to clusters within a few seconds after encountering the aqueous building block solution in the first cross-section. An increasing agglomeration of the vaterite particles in the droplets is demonstrated in Figure 4a progressing from the red section to the green and finally the yellow section. After gelation of the droplets occurs, the resulting vaterite-containing microgels are transferred into phosphate buffer or water.

Vaterite agglomerates in the microgels are characterized by 3D confocal laser scanning microscopy. By incubation in a dye solution of sulforhodamine B and calcium-selective tetracycline, the vaterite particles and the microgels are distinguishable due to the special affinity of sulforhodamine B to the polymer scaffold and tetracycline to the vaterite particles. In Figure 4b, vaterite clusters stained in blue and microgels stained in red and an overlay of the two images is shown. By confocal laser scanning microscopy (transmission path), vaterite particles are also recognizable as dark spots in the microgels (Figure 4c).

Metastable vaterite may transform to the thermodynamically more stable calcite or aragonite during the microfluidics studies. To determine if this is the case, the stability of vaterite in the microgels is confirmed by confocal Raman spectroscopy, since vaterite and the other calcium carbonate modifications as calcite

and aragonite are Raman active compounds. The successful verification of the vaterite modification is depicted in Figure 4, where in Figure 4d, a bright-field image of a microgel section containing vaterite agglomerates stored in water is shown. The image shown is made 48 h after gelation of the microgel. In Figure 4e, the confocal Raman image from the black squared area of the bright-field image is shown. The red area shows the vaterite agglomerates, and the blue area shows the microgel fragment, stored in water. The Raman spectrum obtained after hyperspectral analysis of the measured microgel section including vaterite agglomerates is shown in Figure 4f. The blue spectrum corresponds to the combined signals of the microgel PEG backbone and water. Due to the high impact of water in the microgels, a separation into two single spectra is not possible. The red spectrum presents the characteristic bands of vaterite, which corresponds to the symmetric stretching mode $\nu_1$ at 1090 and 1075 $cm^{-1}$, the in-plane bending motion $\nu_4$ at around 744 $cm^{-1}$, and the lattice modes at 305 and 120 $cm^{-1}$.[10,12] This spectrum is obtained after subtracting the combined spectrum of PEG and water from the mean spectra of the red area and shows the meta-stable vaterite modification, successfully encapsulated in the microgels (for details see Figure S4, Supporting Information).

#### 2.2.3. Transformation of Vaterite to HCA

For the assessment of the in vitro bone-like HCA forming ability of vaterite embedded in the polymer matrix, vaterite-containing gels are immersed in Dulbecco's phosphate-buffered saline (DPBS) and analyzed by FT-IR spectroscopy. The same measurements are also performed with the polymer matrix and with pure vaterite particles as a control. Respective IR-spectra are depicted in **Figure 5**, where measurements before the immersion in phosphate buffer and after 48 h of immersion are shown. The IR-spectra of the polymer matrix (Figure 5a) show no changes after 48 h of incubation in DPBS, while the spectra of vaterite particles (Figure 5b) record an increase of $PO_4^{3-}$ band intensity (non-degenerate symmetric P–O stretching mode at 963 $cm^{-1}$ and the triply degenerate antisymmetric P–O stretching mode at 1024 $cm^{-1}$).[12,19] Additionally, the typical vibrational frequencies of the $CO_3^{2-}$ bands at 1487–1411, 1090, 877, and at 744 $cm^{-1}$, are shown in both spectra. These results indicate the transformation of vaterite to HCA and agree to previous findings of Schröder et al.[12,19]

The IR-spectra of vaterite-containing gels (25 wt%) are shown in Figure 5c, whereby the spectra of the sample before immersion in DPBS mainly display the frequencies of the polymer scaffold, but also two characteristic bands of vaterite at 877 and at 744 $cm^{-1}$. After 48 h of incubation in DPBS, the spectra change. The intensity of the polymer frequencies is mainly decreased, which is caused by hydrolysis-sensitive ester groups in the polymer network. Due to the vaterite-caused increased basicity of DPBS, the polymer degradation is accelerated and makes a view of the mineral spectra possible, which is comparable to that of pure vaterite after 48 h of incubation in DPBS. This analysis indicates a vaterite transformation in the polymer matrix to HCA and makes the vaterite/PEG composite material a suitable candidate for further investigations on the mineral level.

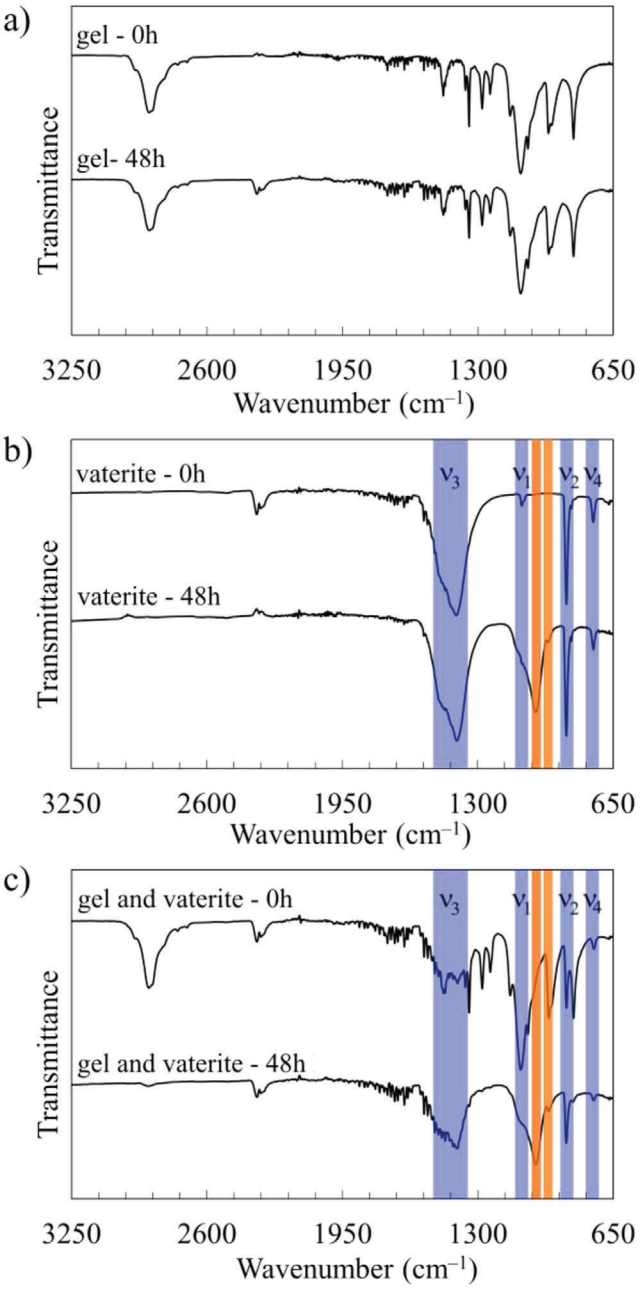


**Figure 5.** Transformation of vaterite particles embedded within the polymer matrix to HCA at physiological conditions. FT-IR-spectra of a) the PEG polymer matrix, b) pure vaterite particles (normalized to $\nu_2$), and c) vaterite particles embedded in the polymer matrix, each before and after 48 h incubation in DPBS.

### 2.3. Gel Composition versus Cellular Viability

#### 2.3.1. Endotoxin and Toxicity Testing of Gels

To determine the cell- and biocompatibility of the gels, endotoxin and toxicity tests are done. For the endotoxin assay, gels and extracts from gels ([4-arm PEG-thiol 10 000 g $mol^{-1}$ (10K)/linear PEG-acrylate 5000 g $mol^{-1}$ (5K)] composition with a mean mass

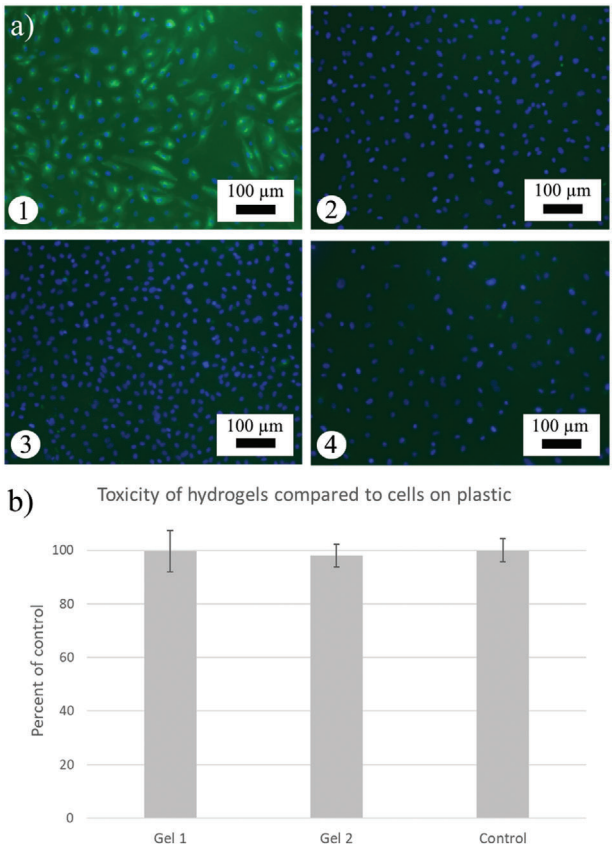


**Figure 6.** Endotoxin and toxicity testing of gels of type [4-arm PEG-thiol 10 000 g mol$^{-1}$ (10K)/linear PEG-acrylate 5000 g mol$^{-1}$ (5K)]. a) Evidence of endotoxin by E-selectin staining of HUVEC cells cultured on plastic (1, 2) and exposed to gels (3) or supernatant extract from the gels (4). A positive control is shown in (1), where HUVEC cells are exposed to 1 µg mL$^{-1}$ endotoxin (LPS) after 24 h incubation on plastic. The intense green fluorescence indicates the presence of E-selectin (using E-selectin as a first antibody and anti-mouse Alexa Fluor 488 as a second antibody), whereby the dye Hoechst 33342 is used to stain the cell nuclei (blue). The control, (2), as well as cells exposed to the gel or extracts from the gel (3 and 4, respectively) show no green staining and indicate endotoxin-free materials. Similar results are observed with two different donors of HUVECs. b) Relative metabolic activity of cells growing on gels compared to cells growing on cell culture plastic (control), by examining the conversion of resazurin to resorufin. The cells growing on two gels exhibited nearly an identical metabolic activity for the reduction of resazurin after 24 h compared to the control cells growing on cell culture plastic set to 100%. Two different donors for HUVEC are used (mean ± SD; $n = 8$).

concentration of 160 g L$^{-1}$) are added to HUVEC cells in culture, whereby no induction of E-selectin is observed. Based on previous studies showing that the induction of the cell-adhesion molecule E-selectin by endotoxin is a highly sensitive method for the detection of endotoxin in biomaterials, it is clear that the precursor polymer synthesis methods used for the formation are sufficient for the production of endotoxin-free gels.[20,21] In **Figure 6**a, respective images of HUVEC cells cultured on plastic are shown, and the dye Hoechst 33 342 is used to stain the cell nuclei (blue). In (1), cells are exposed to 1 µg mL$^{-1}$ endotoxin (LPS), which results in an intensely green stain that indicates the presence of E-selectin; (2) is an untreated control of HUVEC cells, while (3) and (4) are cells exposed to the gel or extracts from the gel. The absence of green staining in (3) and (4) indicates no induction of E-selectin and therefore the absence of endotoxin in the test sample.

The viability of cells growing on two gels ([4-arm PEG-thiol 10 000 g mol$^{-1}$ (10K)/linear PEG-acrylate 5000 g mol$^{-1}$ (5K)] composition with a mean mass concentration of 300 g L$^{-1}$) is compared to the same amount of cells growing on plastic (control experiment). GFP-marked osteoblast cells (MG-63 GFP) are used since osteoblasts are responsible for the production of extracellular matrix (e.g., collagen) in metabolic bone regeneration processes and has been extensively used as a model cell line for osteoblast studies on biomaterials.[12] The metabolic activity of the cells is assayed after 24 h by examining the conversion of resazurin to resorufin. Only viable, metabolically active cells can carry out this conversion. As can be seen in Figure 6b, cells on the gels exhibit nearly the same amount of metabolic activity after 24 h as the cells on plastic, and therefore, the gels exhibit no toxic effect on the cells.

### *2.3.2. Gel Elasticity*

In most cases, endogenous cells will grow into implanted biomaterials, but the preclinical development requires an optimization of the materials that is usually accomplished with ex vivo and in vivo experiments. Since in vivo experiments are complex, time consuming, and expensive, the in vivo studies can be mimicked ex vivo by examining cells. This requires that the gel elasticity be optimized to maximize the viability of the cells.

To achieve a general understanding of the cell behavior in different polymer-network mesh-sized scaffolds, MG-63 GFP are encapsulated by microfluidics in three different polymer networks that differ from each other in terms of the polymer-network mesh size and consequently in the gel stiffness or softness. A focus is placed on the influence of the gel mechanical strength and gelation time on the cell viability.

To examine the influence of the variation of the polymer-network mesh size, the molar mass of the 4-arm PEG-thiol precursor polymer is kept constant at 10 000 g mol$^{-1}$ (10K), whereas the molar masses and thereby the length of the linear PEG-acrylate precursor polymers are varied from 2000 g mol$^{-1}$ (2K) over 5000 g mol$^{-1}$ (5K) to 7500 g mol$^{-1}$ (7.5K) (**Table 1**). The molar concentration of the precursor polymers in diverse solvents (and thus the molar concentration of their reactive end groups) is kept constant at a ratio of 1:2 (4-arm PEG-thiol to linear PEG-acrylate), whereas their respective mass concentrations increase within the three systems.

The network stiffness and gelation times of the three systems are analyzed by time-dependent rheology measurements of macrogels. The resulting curves are shown in **Figure 7**, where the storage modulus, $G'$, and the loss modulus $G''$, are plotted against time. The crossing points serve as an indication of the gelation time ($t_g$), and the terminal storage modules ($G_g'$) denotes the polymer gel stiffness, whereby the plateau storage modulus $G'$ is generally connected to the number density of elastically effective chains in the gel, $\nu_{eff,1}$, by the phantom network model

**Table 1.** Polymer network compositions and rheological measured data.

| | $M$ [kDa] | $c_{Prec}$ [mol $L^{-1}$] | $c_{Prec}$ [g $L^{-1}$] | $t_{buffer}$ [min] | $G'_{buffer}$ [kPa] | $\xi_{buffer}$ [nm] | $t_{mixture}$ [min] | $G'_{mixture}$ [kPa] | $\xi_{mixture}$ [nm] |
|---|---|---|---|---|---|---|---|---|---|
| 4-arm PEG-thiol | 10 | 0.03 | 300 | 29 | 15.7 ± 0.8 | 6.4 | 11 | 20.9 ± 3.6 | 5.8 |
| Linear PEG-acrylate | 2 | 0.06 | 120 | | | | | | |
| 4-arm PEG-thiol | 10 | 0.03 | 300 | 15 | 29.9 ± 3.1 | 5.2 | 4 | 26.6 ± 3.9 | 5.4 |
| Linear PEG-acrylate | 5 | 0.06 | 300 | | | | | | |
| 4-arm PEG-thiol | 10 | 0.03 | 300 | 11 | 28.7 ± 1.4 | 5.2 | 4 | 30.3 ± 3.9 | 5.2 |
| Linear PEG-acrylate | 7.5 | 0.06 | 450 | | | | | | |

The network compositions are based on the molar masses of the precursor polymers ($M$), and the molar, and mass concentrations ($c_{Prec}$) in diverse solvents. Storage and loss modulus crossing points in buffer ($t_{buffer}$) and in a mixture of phosphate buffer/DMEM (1% Gl, 10% FBS, 1% P/S) at a ratio of 6:1 ($t_{mixture}$) as well as the final network storage moduli after 5 h of reaction time ($G'_{buffer}$ and $G''_{mixture}$) are obtained by rheology. Respective polymer-network mesh sizes ($\xi_{buffer}$ and $\xi_{mixture}$) are calculated by the phantom network model.

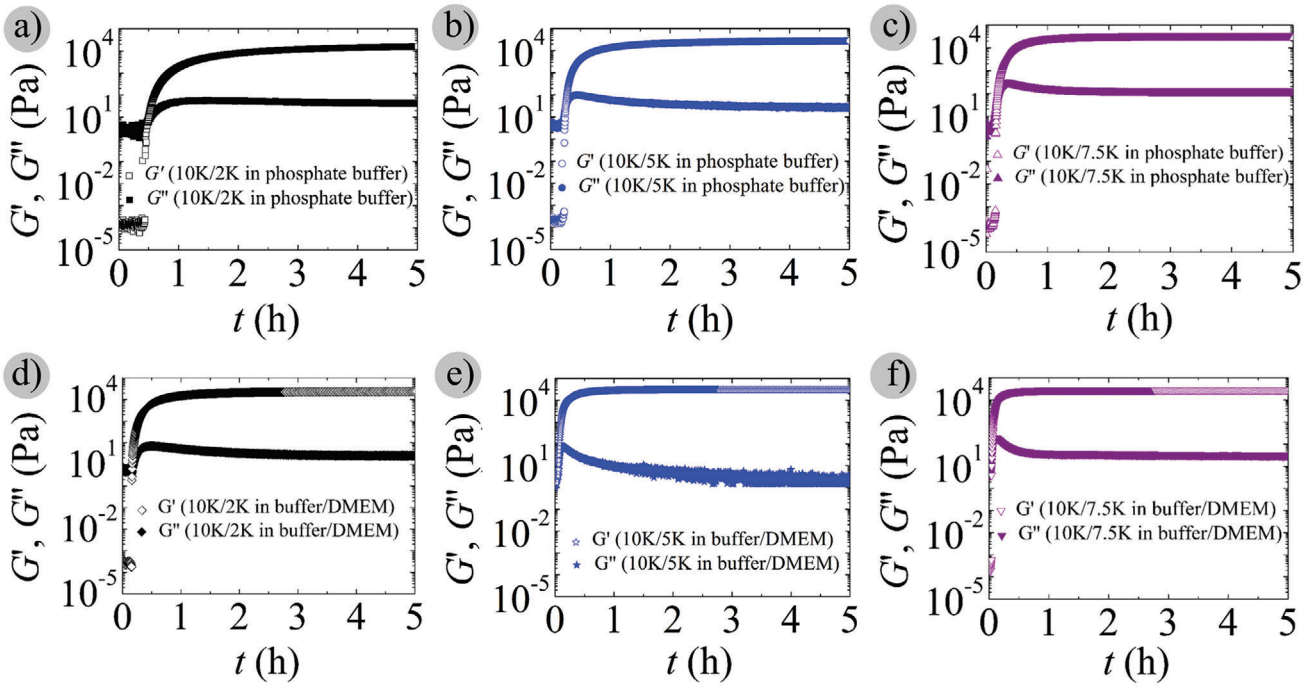


**Figure 7.** Dependency of cell-viability on the scaffolding gel elasticity: Time-dependent storage and loss moduli over time for selected 4-arm PEG-thiol/linear PEG-acrylate network compositions in phosphate buffer (a–c, at the top) and in a phosphate buffer/DMEM mixture at a ratio of 6:1 (d–f, at the bottom). Black symbols: 10K/2K composition (G′ (□), G″ (■) and G′ (◇), G″ (◆)); blue symbols: 10K/5K composition (G′ (○), G″ (●) and G′ (★), G″ (★)); purple symbols: 10K/7.5K composition (G′ (△), G″ (▲) and G′ (▽), G″ (▼)).

($A \cdot \nu_{eff,1} = G'/(RT)$). In this formula, $R$ is the gas constant, $T$ the temperature, and $A = 1 - (2/f)$ is a structure factor, with $f$ the functionality of the cross-links (here, $f = 4$).[22]

Measurements are performed in a phosphate buffered solution as a standard, as well as in a mixture of phosphate buffer and DMEM (1% Gl, 10% FBS, 1% P/S) at a ratio of 6:1. Since disulfide formation as a side reaction to the Michael addition is more dominant in the DMEM culture medium than in the phosphate buffer, experiments are performed in a mixture of phosphate buffer and DMEM (1% Gl, 10% FBS, 1% P/S). The respective values are listed in Table 1, where buffer and mixture represent the measurements in phosphate buffer or in the mixture medium.

*Discussion of the Gelation Time*: In phosphate buffer, the 4-arm PEG-thiol/linear PEG-acrylate 10K/2K (Figure 7a) (G′ (□), G″ (■)) composition gels after 29 min. In contrast, the 10K/5K (Figure 7b) (G′ (○), G″ (●)) composition gels within 15 min and is thus twice as fast as the 10K/2K composition. Furthermore, the 10K/7.5K (Figure 7c) (G′ (△), G″ (▲)) composition gels within just 11 min. Therefore, the gelation time decreases with increasing molar mass of the linear PEG-acrylate (2K, 5K up to 7.5K). This is because the hydrodynamic radius increases in the same row, making the reactive ends of the precursor polymers more likely to find and react with the reactive groups of the PEG-thiol components at increasing size of the linear PEG-acrylate.[22] Also, a greater hydrodynamic radius comes along with a lower

probability of loop-type reaction of both ends of the same linear precursor with two extremities of the same star precursor, which consumes these precursors without contributing to actual network formation and this delays the formation of a percolated network. Almost the same sequence is observed in the phosphate buffer/DMEM mixtures, although at a faster rate. The 4-arm PEG-thiol/linear PEG-acrylate 10K/2K (Figure 7d) ($G''$ (◇), $G'$ (◆)) composition gels after 11 min, whereas the 10K/5K (Figure 7e) ($G'$ (★), $G''$ (★)) composition and the 10K/7.5K (Figure 7f) ($G'$ (▽), $G''$ (▼)) composition gels within just 4 min. Here, the more alkaline pH value of the phosphate buffer/DMEM mixture in comparison to the pH of the pure phosphate buffer is most likely responsible for the overall accelerated reaction rate. It is also possible that there is an overall larger radius of gyration of the linear building block in the phosphate buffer/DMEM mixture than in phosphate buffer, due to the additional salts and amino acids in DMEM, thereby leading to the faster gelation.

*Discussion of the Gel Stiffness*: Comparison of the terminal storage moduli $G'$ indicates differences between the networks. In phosphate buffer, the 10K/2K (Figure 7a) ($G'$ (□), $G''$ (■)) composition shows the lowest storage modulus ((15.7 ± 0.8) kPa) and is therefore the softest network compared to the others. The 10K/5K (Figure 7b) ($G'$ (○), $G''$ (●)) and the 10K/7.5K (Figure 7c) ($G'$ (△), $G''$ (▲)) compositions show storage moduli of (29.9 ± 3.1) and (28.7 ± 1.4) kPa. The increase in the network strength between these three systems from (15.7 ± 0.8) to (29.9 ± 3.1) and (28.7 ± 1.4) kPa is due to the different size of the PEG-acrylate building blocks. The smaller the radius of gyration, the more likely is the occurrence of looping defects in the network, and hence, these networks are softer. This agrees with the longer time it takes for these precursors to actually form a gel, as just discussed above. Similar results are obtained with the phosphate buffer/DMEM mixture (10K/2K: (20.9 ± 3.6) kPa, 10K/5K: (26.6 ± 3.9) kPa, 10K/7.5K: (30.3 ± 3.9) kPa) (Figure 7d–f) and demonstrates that the culture medium has little effect on the final gel stiffness.

The nanoscopic mesh sizes, $\xi$, of the polymer networks are calculated using the number density of elastically effective chains from the phantom network model $A \cdot \nu_{\mathrm{eff},1} = G'/(RT)$ from the moduli. The product of the structure factor $A$ and the number density of elastically effective chains on the left side, $A \cdot \nu_{\mathrm{eff},1}$, equals the number density of elastically effective cross-links $\nu_{\mathrm{eff},2}$ [mol $L^{-1}$]. Multiplication of $\nu_{\mathrm{eff},2}$ with the Avogadro constant $N_A$ yields the absolute number of effective cross-links per liter, and the mean distance of these cross-links, that is, the mesh size $\xi$, is obtained from the cube-root of the inverse of that value: $\xi = (1/(\nu_{\mathrm{eff},2} \cdot N_A))^{1/3} = (RT/(G' \cdot N_A))^{1/3}$. In this calculation, $R$ is the gas constant, $T$ the temperature at which $G'$ was measured, $N_A$ the Avogadro constant, and $G'$ the measured storage modulus of each network, here at a measurement frequency of 6.28 rad $s^{-1}$ (Table 1). Altogether, the mesh sizes calculated in this manner do not differ from each other: both in the phosphate buffer and in the phosphate buffer/DMEM mixture, the mesh sizes of the 10K/5K and 10K/7.5K systems are estimated to be approximately 5.2 or 5.4 nm, whereas the mesh sizes of the 10K/2K system are slightly larger in the phosphate buffer (6.4 nm) and in the phosphate buffer/DMEM mixture (5.8 nm). This is a reflection of the same trends in the moduli, from which the mesh sizes are actually calculated.

In summary, the three polymer systems show storage moduli of similar magnitude, corresponding to similar network mesh sizes, but with differences in the cross-linking time of the precursor polymers.

### 2.3.3. Gel Permeability

To independently probe the polymer-network meshes, fluorescence correlation spectroscopy (FCS) is used to measure the permeability of small and mesoscopic probes through the gels. This study also mimics the diffusive permeation of nutrients and metabolites in the gels in cases where cells are encapsulated in order to determine how efficient the transport of species of this size and molar mass occurs to and from cells. To determine this, gel samples of type 10K/2K, 10K/5K, and 10K/7.5K are prepared and incubated in a dye solution for several hours. The FCS measurements are performed on macrogels rather than on microgels. Since the reaction conditions in the production of the micro- and macrogels are similar, it is predicted that very similar network structures will be generated in either form. Therefore, the diffusion coefficients measured in the macrogels can be applied to the microgels as well.

Sulforhodamine B is chosen as a surrogate for low-molar-mass components of the culture medium (e.g., salts and amino acids). Rhodamine has a diffusion coefficient $D$ of 440 μm$^2$ $s^{-1}$ in aqueous solutions,[23] and this is used to calculate the hydrodynamic radius $R_H$ of 0.5 nm using the Stokes–Einstein equation ($R_H = k_B T/6\pi\eta D$), with $k_B$ the Boltzmann constant, $T$ the room temperature, and $\eta$ the viscosity of the medium (essentially, identical to water). In contrast, bovine serum albumin (BSA) labeled with tetramethyl rhodamine is chosen as a surrogate for larger molecules in the culture medium (e.g., proteins), as BSA is a major protein in cell culture medium with a measured diffusion coefficient $D$ of 204 μm$^2$ $s^{-1}$ in aqueous solutions and a calculated hydrodynamic radius of 1.1 nm. In the three specific networks, FCS measurements show diffusion coefficients of similar magnitude for both sulforhodamine B and dye-labeled BSA. Compared to free sulforhodamine B in phosphate buffer (440 μm$^2$ $s^{-1}$),[23] the diffusion coefficients in the networks are four to five times slower ($D_{10K/2K}$ = (105 ± 15) μm$^2$ $s^{-1}$, $D_{10K/5K}$ = (93 ± 8) μm$^2$ $s^{-1}$, $D_{10K/7.5K}$ = (88 ± 10) μm$^2$ $s^{-1}$), whereas compared to free dye-labelled BSA (204 μm$^2$ $s^{-1}$), the diffusion coefficients are two times slower in the networks ($D_{10K/2K}$ = (120 ± 27) μm$^2$ $s^{-1}$, $D_{10K/5K}$ = (118 ± 19) μm$^2$ $s^{-1}$, $D_{10K/7.5K}$ = (76 ± 6) μm$^2$ $s^{-1}$). These lowered diffusion coefficients indicate an inhibited diffusion of the substrate due to the network cross-linkings and chains. Nevertheless, a sufficient nutrient exchange between the gels and the surrounding medium up to a substrate hydrodynamic radius of 1.1 nm is possible.

### 2.3.4. Encapsulation of Cells

The influence of the gel properties on the viability of MG-63 GFP is analyzed by encapsulation into microgels. For this purpose, the microfluidic device shown in Figure 1 (on the left and on the right side) is used. Microgel production occurs after injection of aqueous 4-arm PEG-thiol and linear PEG-acrylate precursor

polymer solutions (dissolved in phosphate buffer) each at the first junction of the microfluidic device, along with cells suspended in DMEM (1% Gl, 10% FBS, 1% P/S) and 15% OptiPrep acting as a density-increasing compound to avoid deposition of the cells in the microfluidic experiment. After gelation and purification, cell-containing microgels of the 10K/5K type are incubated in DMEM (1% Gl, 10% FBS, 1% P/S) at physiological conditions (37 °C, 5% $CO_2$, and humidity) over a period of 2 weeks (**Figure 8**a). During the first 7 days, cells are centered in the microgels and form clusters, while the polymer-gel specimen swells due to the hydrolysis of ester groups in the polymer network. The increase of the degree of network swelling is illustrated by white dashed lines around the microgels. After complete degradation of the microgels (after about 7–8 days), cloud-like cell clusters are observed in the culture medium. These clusters eventually settle at random points on the culture dish surface, adhere, and proliferate, seen as cells growing out of the clusters (day 9). With time, cells continue to increase in numbers until at least day 14. This observation demonstrates a high viability of cells that are encapsulated for at least 7 days within the 10K/5K polymer network, and these cells are able to attach and proliferate after gel degradation, as evidenced by their growth on the cell culture dish surface.

In parallel to the microfluidic experiment, the viability of the cells is monitored in control experiments. For this purpose, the cells are seeded on plastic, and their growth is followed over a period of 7 days. The visualization of the cell growth is performed by 2D confocal microscopy, whereby an increasing intensity of green fluorescence indicates increasing cell growth. Figure 8b shows one experiment at days 1, 3, and 7.

Cells are also encapsulated in the 10K/2K and 10K/7.5K networks. Cells in the 10K/2K microgels behave similar to cells encapsulated in the 10K/5K system (Figure 8c). These cells form cellular clusters that adhere to the cell culture dish after gel degradation. In contrast, the encapsulated cells in the 10K/7.5K network (Figure 8d) do not survive. In this experiment, cellular clusters are not observed after degradation of the microgels; however, some isolated, rounded-up single cells are observed that do not adhere to the cell culture dish. The viability of the cells is also monitored in control experiments (Figure 8e,f)

Differences in the cellular viability between both polymer systems 10K/2K and 10K/7.5K are probably based on differences in the ability of the cells to form cell–cell contacts. Since PEG is an antifouling material and resistant against protein adsorption from the environment, cells are not able to adhere to that material.[24] Instead, they form a round sphere-like morphology and aggregate to cell clusters through specialized protein complexes, like E-cadherin, integrin, or ECM proteins.[25] This can be observed in the 10K/2K and 10K/5K networks, where the cells interact spatially and form clusters, whereas the cells in the 10K/7.5K system remain isolated over the entire encapsulation period. As cell–cell interaction is an important parameter of cellular viability,[26] this might be the cause for survival differences in the networks.

The inhibition of cell–cell contacts in the 10K/7.5K microgels may be based on differences in the gelling time, the elasticity of the polymer network, and the viscosity of the precursor polymer solution. The 10K/5K system and the 10K/7.5K system both require approximately 4 min to gel in the hybrid mixture of phosphate buffer and DMEM, respectively, and the elasticity

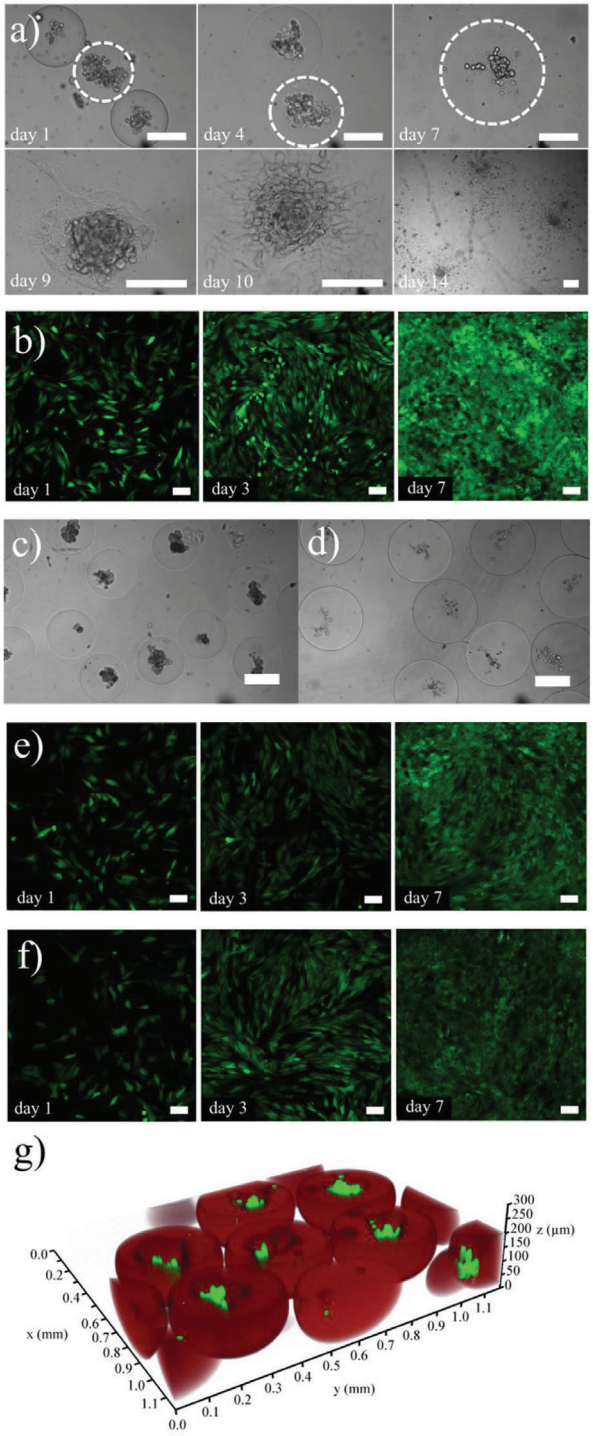


**Figure 8.** Cell-containing microgels. a) Monitoring of the cell viability in 10K/5K microgels is performed by light microscopy imaging over a period of 2 weeks. b) Control test of the experiment with 10K/5K microgels monitored by 2D confocal microscopy. Increasing green fluorescence of GFP expressing cells indicates cell proliferation. c) Light microscopy imaging of type 10K/2K and d) 10K/7.5K microgels containing cells. e) Control test of the experiment with 10K/2K microgels and f) 10K/7.5K microgels. g) 3D confocal microscopy of MG-63 GFP cells (green fluorescence) in microgels of type 10K/2K, incubated in a sulforhodamine B/phosphate buffer solution (red fluorescence). Scale bars: 100 µm.

of both polymer gel systems has been found to differ only marginally ((26.6 ± 3.9) and (30.3 ± 3.9) kPa). Despite this similarity, however, the cell viability in these two systems differ substantially. The reason may be due to the different viscosities of the precursor polymer solutions. In the 10K/5K system, the cells are embedded in a 300 g $L^{-1}$ precursor solution with a linear-precursor polymer molar mass of 5000 g $mol^{-1}$, whereas in the 10K/7.5K system, they are embedded in a 375 g $L^{-1}$ solution with a linear-precursor polymer molar mass of 7500 g $mol^{-1}$. Both the higher concentration and polymer molar mass in the 10K/7.5K system as compared to the 10K/5K entails a higher solution viscosity, which impairs cellular motion. If the gelation is then faster than the time that it takes for cells to come into physical contact with one another in that viscous surrounding, they are fixed at isolated positions in the polymer network, as it is the case in the 10K/7.5K system, thereby preventing them from forming cell clusters.

Next to the precursor polymer viscosity, the gelling time is more influential in the 10K/2K system compared to the 10K/5K and the 10K/7.5K systems. In the 10K/2K system, the low precursor polymer concentration of only 210 g $L^{-1}$, along with the lower linear-polymer molar mass of 2000 g $mol^{-1}$ entails a low viscosity and therefore promotes cell migration in the precursor–gel droplets. In addition, the 11-min gelling time in the phosphate buffer/DMEM mixture is two and a half times longer than the gelling times of the 10K/5K and the 10K/7.5K systems, which also allows for more distant cell migration in the pre-gel stage. As a result, the cells have more time and can migrate with a higher mobility in the pre-gel droplets to form clusters by the expression of junction proteins before gelation occurs.

Figure 8g shows the encapsulated cells in a microgel network of the 10K/2K type, visualized by 3D confocal imaging. For this purpose, the cell containing microgels are incubated in a solution of red-fluorescent sulforhodamine B. The red dye molecules adhere to the polymer network allowing visualization of the microgels and the green fluorescence stems from the GFP expressing cells. As can be seen, the cells are located in the center of the microgels. This is achieved by shaking of the cell containing droplets during the microfluidic steps, thereby preventing sedimentation of the cells in the templates.

### 2.4. Cell- and Vaterite-Containing Microgels

As a next step toward material development for ex vivo tests, co-encapsulation of both cells and vaterite particles is performed, using the modified microfluidic device shown in Figure 1 (middle scheme). Besides the injection of the two polymeric building blocks (4-arm PEG-thiol and linear PEG-acrylate, solved in phosphate buffer), the independent encapsulation of both, vaterite particles suspended in ethylene glycol (3.4% w/v), as well as the cell suspension of osteoblasts (MG-63 GFP) and DMEM in droplets, is made possible. While the two polymeric building blocks react in a thiol–ene Michael addition and form 3D polymer networks, the injected cells form cell clusters and vaterite particles agglomerate to larger granules distributed in these networks. Respective cell- and vaterite-containing microgels are observed with 2D confocal microscopy over a period of several days as shown in **Figure 9**a (above). Since the (4-arm PEG-thiol

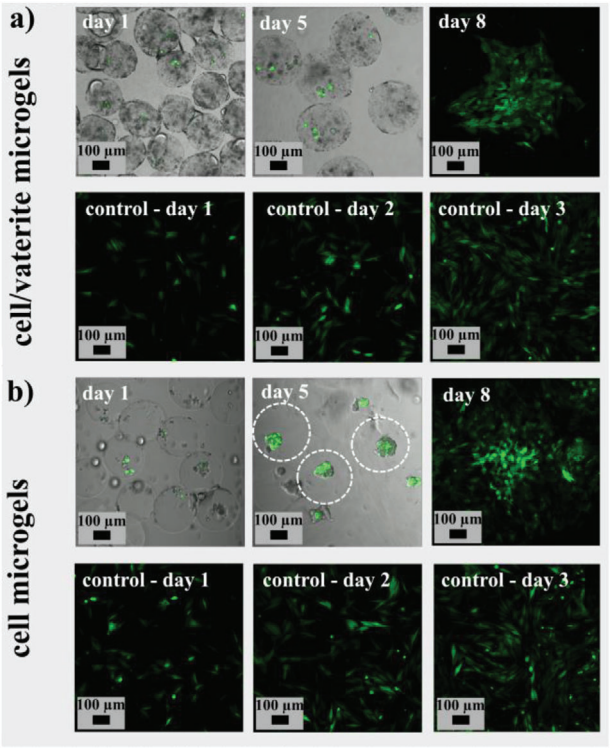


**Figure 9.** Viability of cells in vaterite-containing and vaterite-free microgels. a) MG-63 GFP cells encapsulated in vaterite-containing microgels of the 10K/2K type and b) in microgels of the 10K/2K type without further vaterite particle encapsulation. Cell viability is monitored in both experiments by 2D confocal microscopy over a period of 8 days. Depicted are days 1 and 5, where a superposition of transmission and fluorescence paths is shown, while day 8 is only shown in the fluorescence path. A control experiment is also performed by 2D confocal microscopy over a period of 3 days. Scale bars: 100 µm.

10 000 g $mol^{-1}$ [10K]/linear PEG-acrylate 2000 g $mol^{-1}$ [2K]) polymer composition is chosen, a high cell viability is ensured, which is investigated by microgel incubation in DMEM (1% Gl, 10% FBS, 1% P/S) at physiological conditions (37 °C, 5% $CO_2$, and humidity). The images of day 1 and day 5, respectively, show microgels with vaterite agglomerates visible as dark spots (transmission path), superimposed with the green fluorescence of cells expressing GFP (fluorescence path). Since the degree of microgel swelling increases with time due to hydrolysis-sensitive ester groups in the polymer network, the microgel diameter increases from day 1 to day 5, until complete gel degradation after about 7 days. Additionally, cells in the microgels form clusters by cell–cell interactions and settle after degradation of microgels at random points on the culture dish surface and adhere and proliferate. This is shown in the image of day 8, where the green fluorescence indicates high viable layer of adherent cells.

In comparison, the same number of cells as in the experiment above are encapsulated in the (4-arm PEG-thiol 10 000 g $mol^{-1}$ [10K]/linear PEG-acrylate 2000 g $mol^{-1}$ [2K]) polymer system, using the microfluidic device shown in Figure 1 (left and right side of the scheme) without further vaterite encapsulation. The respective microgels are also observed with 2D confocal microscopy, while incubating in DMEM (1% Gl, 10% FBS, 1% P/S)

at physiological conditions (37 °C, 5% $CO_2$, and humidity) over a period of several days, as shown in Figure 9b (above). While the microgel diameters increase during the incubation period (day 1 to day 8) comparable to these of vaterite- and cell-containing microgels, cell clusters are formed by cell–cell interactions as well. Microgels degrade after approximately 7 days, and the released cell clusters adhere to the plastic and proliferate, which indicates a high cell viability (day 8).

In parallel to both microfluidic experiments, the general viability of the cells is monitored in triple control experiments over a period of 3 days. In Figure 9a,b (below), one experiment is shown each after 24, 48, and 72 h of incubation. Visualization of the cell growth is achieved by 2D confocal microscopy, and the increasing intensity of green fluorescence indicates increasing cell growth.

In summary, cells encapsulated in both microgels with and without vaterite particles survive the microfluidic experiments and remain in the gels over a period of 7 days. This indicates that the polymer model system described in this study is highly suitable for further studies of bone tissue regeneration. Differences of cell growth are marginal, most likely due to differences in the gelation time of precursor polymers in droplets. In vaterite-free microgels, encapsulated cells are present as agglomerates in the microgels from day 1 and grow into large clusters during the 8-day incubation period in culture medium. These agglomerates consist of many cells. In vaterite- and cell-containing microgels, encapsulated cells are mostly present as smaller agglomerates up to single cells beginning at day 1. When vaterite particles are encapsulated, a slight increase of pH is observed in the reaction solution in the droplets, which decreases the reaction time of polymer-network formation. Cells in the droplets are therefore impaired to form contacts and such remain as small agglomerates or single cells. Nevertheless, with increasing incubation time in culture medium, the cells grow into larger clusters. This is probably enabled by the small modulus of the (10K/2K) system ((20.9 ± 3.6) kPa), which also decreases with increasing incubation time due to hydrolysis sensitive ester groups in the network. The resulting lower constriction to the encapsulated cells enables them to grow more easily. An additional favorable influence will probably have vaterite particles in the gels, since they are highly compatible for osteoblasts and promote cell growth as proven in previous studies.[12]

### 2.5. Microgel Degradation

An additional feature of the polymer networks used in this study are the hydrolysis-sensitive ester groups that promote polymer degradation in aqueous environments. After cleavage of these ester groups, there is a loss of network points in the polymer network and thereby an increase in the degree of swelling over time until complete degradation of the microgels occurs.

Investigation of the pH dependence of the polymer degradation is performed with microgels of the 10K/5K type by incubation in phosphate buffer at pH 5.0, 7.2, and 9.0 at room temperature. At acidic and neutral pH, no swelling is observed for 40 days (△,○). By contrast, microgels in alkaline buffer solution (pH 9.0) show a marked ongoing swelling (□) and decompose completely after approximately 1 month. The increase of the degree of swelling of the gels in alkaline buffer solution is also illustrated

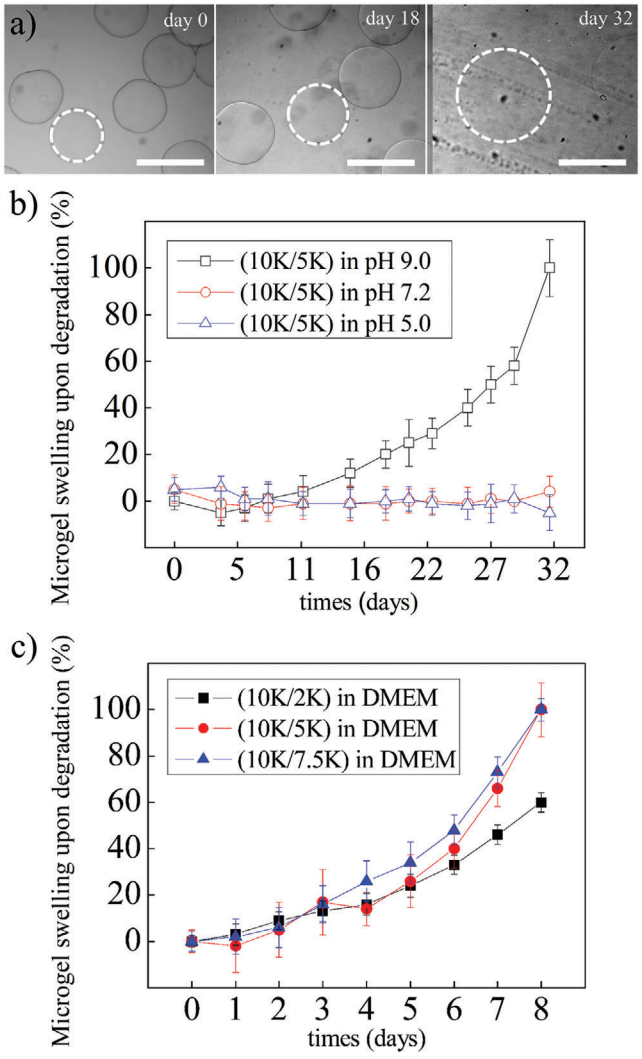


**Figure 10.** Degradation of microgels. a) Stability of gels of type 10K/5K in phosphate buffer at pH 9.0 and room temperature, as observed over a period of 32 days. The increase of the degree of swelling of the gels is illustrated by the white dashed outlines. b) Time-dependent microgel swelling in phosphate buffers at various pH values of 10K/5K microgels (all measurements are performed at room temperature; pH 9.0 (□), pH 7.2 (○), pH 5.0 (△)). c) Time-dependent microgel swelling in culture medium (DMEM with 1% Gl, 10% FBS, and 1% P/S) at physiological conditions (5% $CO_2$ and 37 °C) with microgels of the (10K/2K) (■), (10K/5K) (●), and (10K/7.5K) (▲) type. Gels show degradation in nearly 1 week. The measured data are linked by lines to guide the eye. Scale bars in panel (a): 300 µm.

by the white dashed outlines in **Figure 10**a (at days 0, 18, and 32). The respective swelling curves are depicted in Figure 10b. Since the goal is to use the gel capsules for biomedical applications, swelling measurements are also carried out in culture medium (DMEM with 1% Gl, 10% FBS, and 1% P/S) at physiological conditions (5% $CO_2$ and 37 °C). Therefore, microgels of type 10K/2K, 10K/5K, and 10K/7.5K are incubated in the cell culture medium for several days. The respective swelling curves are depicted in Figure 10c. Compared to microgels stored in alkaline phosphate buffer at room temperature, microgels stored in cell culture

medium at physiological conditions decompose at a higher rate (within 1 week). Reasons for the faster decomposition of the microgels in the culture medium at physiological conditions compared to phosphate buffer at room temperature are most likely due to the elevated temperature (37 °C instead of room temperature) and additional substances such as amino acids and proteins in the cell culture medium. The accelerated degradation kinetics of microgels in the cell culture medium is considered to be an advantage, as it enables a rapid in situ vaterite particle release in pharmacological experiments. All three polymer systems (10K/2K, 10K/5K, and 10K/7.5K) show similar degradation kinetics (■, ●, ▲), as their number of network points and thus the number of hydrolysis-sensitive ester groups are equal.

## 3. Conclusion

We have developed a system that allows the combination of individual components under various conditions that can be used as a model for the formation of bone-regenerative and cell-containing materials. This model system can be used as an in vitro platform for the study of cellular metabolic processes in bone formation and may provide an in vitro foundation for novel tissue-regenerative therapies. The system uses hydrolysis-sensitive PEG-based model matrixes, formulated to monodisperse microgels to which additional components such as vaterite particles and cells are added using droplet-based microfluidics. The successful encapsulation of vaterite particles in these microgels as calcium precursors is confirmed by confocal Raman spectroscopy, and the transformation of vaterite to HCA is demonstrated using FT-IR spectroscopy measurements. Based on these results, we provide a powerful biopolymer-supported starting point for bone mineral growth and hence a basis for further investigation using this model system for tissue regeneration. Furthermore, osteoblast cells (MG-63 GFP) are successfully encapsulated into the microgels. This is demonstrated by confocal microscopy and cell studies show that these cells remain viable. Cells are present in microgels as agglomerates and show a greater viability than single cells under similar conditions. Rheological experiments demonstrate that the polymer system can be adjusted to form different network mesh sizes and to exhibit different gelation times and viscoelasticity, and that this can all result in differences in cell agglomeration and subsequent cell viability in the microgels. Initial studies with this model system have demonstrated that vaterite and cells can be co-encapsulated into the microgels and that a similar cell viability and high cell-compatibility is observed under these conditions compared to microgel containing only cells but no vaterite. Thus, this model system will be useful for examining and optimizing conditions for mineralization by osteoblasts in a microgel when a bone-forming substrate is available and for delivering bone-forming substrates to a target for tissue regeneration in vivo. The entire vaterite- and cell-containing microgel package becomes a model system for future in vitro and in vivo studies targeting bone tissue-regenerative applications.

## 4. Experimental Section

*Materials*: The precursor polymers 4-arm PEG-thiol 10K and linear PEG-acrylate 2K, 5K, and 7.5K were purchased from JenKEM Technology, USA. The Novec HFE-7500 fluid as well as HFE-7100 are purchased from 3M. Krytox 157-FSH was obtained from DuPont, GIPCO GlutaMAX Supplement and BSA-labelled tetramethylrhodamine from Thermo Fisher Scientific, Optiprep from StemCell Technologies, ethylene glycol from ChemPur, 1*H*,1*H*,2*H*,2*H*-perfluoro-1-octanol, as well as 1*H*,1*H*,2*H*,2*H*-perfluoroctylsilan 97% from Alfa Aesar, and sodium bicarbonate from Roth. The MG-63 GFP osteoblast cell line was obtained from the laboratory of one of the co-authors (RU). All other components such as DPBS-D8537, thionyl chloride, $\alpha$, $\alpha$, $\alpha$-trifluortoluene, tris(hydroxymethylamino-methane), trypsin EDTA solution, DMEM high glucose-D5796, fetal bovine serum-F7524, Penicillin–Streptomycin-P4333, calcium chloride dihydrate, and sulforhodamine B were purchased from Sigma-Aldrich.

*Synthesis of PFPE–Tris Surfactant*: PFPE–Tris was synthesized in a two-step process using a method of Chiu et al.[27] In brief, Krytox 157-FSH (5 g, 0.69 mmol), dissolved in HFE-7100, was treated with thionyl chloride (0.81 g, 6.9 mmol) and stirred in an inert gas atmosphere at 50 °C for 24 h. The resulting mixture was concentrated using cold distillation and then resolved in HFE-7100 (10 mL) and $\alpha$, $\alpha$, $\alpha$-trifluortoluene (6 mL), followed by addition of tris(hydroxymethylaminomethane) (0.084 g, 0.69 mmol) under inert gas atmosphere. A refluxing reaction was conducted at 60 °C for 24 h, and solvents were removed by cold distillation. The crude product was purified by dissolution in HFE-7100 and extraction against water. After cold distillation and vacuum drying, a waxy white product in a yield of 70% was obtained. The PFPE–Tris surfactant was analyzed by FT-IR spectroscopy with an FT/IR-470 instrument (JASCO Analytical Instruments). The results showed a mode at 1683 $cm^{-1}$ that was assigned to the carboxylic acid amide, whereas the carboxylic acid tie of Krytox 157-FSH at 1683 $cm^{-1}$ was no longer observed. This indicated complete conversion of the Krytox 157-FSH. The intensity of both signals was weak due to the large perfluorinated residues.

*Fabrication of PDMS Devices*: Microfluidic devices were produced using photo- and soft lithography. In a first step, silicium wafers (Micro-Chemicals) were spin-coated (WS-650MZ-23NPP13 from Laurell) with a SU-8 2075 photoresist (MicroChem) and irradiated with UV-light (UV-Kub 2 from Kloé) to get negative reliefs of the microfluidic channels that were imprinted on to-scale photomasks. In a second step, PDMS was mixed with a crosslinker (Sylgard 184 elastomer kid from Dow Corning) at a ratio of 10:1 using a Thinky ARE-250 mixing setup, and the mixture was applied to the patterned silicon wafer. After solidifying for 2 h at 65 °C, devices were fabricated by peeling off the resulting reliefed PDMS replica slabs and oxygen plasma bonding (electronic diener Plasma-Surface-Technology) of these onto glass slides. To increase fluorophilicity, the channels were coated with a solution of 2% 1*H*,1*H*,2*H*,2*H*-perfluorooctylsilane in HFE-7100 for a few minutes and this was then removed by air-drying. The resulting channels had a uniform height of 180 µm and a width of 150 µm at the droplet forming cross-junction.

*Synthesis of Vaterite Particles*: Vaterite particles were synthesized using a method previously described.[12,19] Calcium chloride dihydrate (10 mM) was dissolved in ethylene glycol (100 mL) by sonication at 40 °C (Bandelin Sonorex Digitec). Sodium bicarbonate (20 mM) was dispersed in ethylene glycol (100 mL) by mechanical stirring and was added to the calcium chloride solution. The resulting dispersion was sonicated for 25 min at 40 °C. The precursor vaterite solution was analyzed by dynamic light scattering measurements (for details see Figure S3, Supporting Information) to quantify the particle size, which denoted a polydisperse particle size distribution in the range of 200–600 nm. Subsequently, water (100 mL) was added to the vaterite precursor solution and the mixture was sonicated for another 5 min. Precipitated particles were separated from the turbid sol product by centrifugation (9000 rpm; 10 min), washed several times with water and ethanol, and dried under high vacuum. The yield (60%) was determined gravimetrically.

*Vaterite-Containing Microgels*: Droplet templating was carried out with the PDMS device shown in Figure 1 (on the left and right side of the scheme) by connecting the device to four syringe pumps (neMESYS Plugin) via polyethylene tubing (Intramedic Clay Adams Brand PE20) and plastic syringes. The precursor polymers 4-arm PEG-thiol 10 000 g $mol^{-1}$

(300 g $L^{-1}$) and linear PEG-acrylate 5000 g $mol^{-1}$ (300 g $L^{-1}$) were dissolved in phosphate buffer (DPBS) and then equally injected with a flow rate of 75 µL $h^{-1}$, while 5% w/v of vaterite particles in ethylene glycol were injected in the middle channel with a flow rate of 25 µL $h^{-1}$. The vaterite suspension was prepared with a sonotrode (Bandelin Sonopuls), whereby the mixture was homogenized for 10 min at an energy consumption of 19.3 kJ (ice cooling). These three fluids formed a laminar co-flowing stream at the first cross-junction of the microchannel, which was broken to form monodisperse pre-microgel droplets with diameters of approximately 160 µm in the second cross-junction by flow focusing with immiscible HFE 7500, which was injected at a flow rate of 2000 µL $h^{-1}$. To stabilize the resulting droplets, 2 wt% of PFPE–Tris surfactant was also added to the fluorinated oil. Droplets were purified with a 50% solution of 1*H*,1*H*,2*H*,2*H*-perfluoro-1-octanol in HFE7500 in several trituration steps after 30–60 min. After this, the vaterite-containing microgels were transferred into phosphate buffer or water.

*Verification of Vaterite Stability in Microgels*: Confocal Raman microscopy was performed using a Witec 300 alpha R setup. Illumination of the sample was performed using a 532 nm excitation line from a single-mode frequency doubled Nd:YAG laser via a 100-µm single-mode glass fiber. A Zeiss LD EC Epiplan-Neofluar 50x/0.55 objective was used and the laser power at the sample behind the objective was 12 mW. An edge filter was used to separate the Raman signal from the excitation line. Confocality of the Raman signal was achieved via a 50-µm multi-mode fiber glass between microscope and the Raman spectrometer, where the fiber served as a pin-hole. The Raman spectrometer was equipped with a holographic grating of 600 lines per mm. As detector, a Newton Andor EMCCD camera with 1600 × 200 pixels was used. With this configuration, a spectral resolution of about 2 $cm^{-1}$ was obtained. All data sets were analyzed using cluster analysis and non-negative matrix factorization.

*Vaterite Transformation to HCA*: The transformation of vaterite particles to HCA was analyzed using FT-IR spectroscopy. The first measurement was performed without further vaterite incubation in DPBS ($t$ = 0 h). The second measurement was performed after 48 h of vaterite incubation in DPBS (2 g $L^{-1}$) at 37 °C and shaking (150 rpm). Before analysis, the sample was washed three times with water and dried at high vacuum. The analysis of vaterite particles embedded in the polymer gel was carried out as follows: Two gels were prepared mixing 4-arm PEG-thiol precursor polymers 10K and linear PEG-acrylate precursor polymers 5K, solved in phosphate buffer (each with a mass concentration of 300 g $L^{-1}$). 25 wt% vaterite particles (based on the dry precursor polymer total mass) were added and mixed using a sonotrode. After 1 h of gelation time, the first gel was washed three times with water, freeze dried, and analyzed with FT-IR spectroscopy. The second gel was incubated 48 h in DPBS (2 g $L^{-1}$ vaterite in DPBS), then washed three times with water, freeze dried, and analyzed with FT-IR spectroscopy. The analysis of the pure gel ensured analogue to the measurements of gels with vaterite.

*Cell-Containing Microgels*: Droplet templating is carried out with the PDMS device shown in Figure 1 (on the left and right side of the scheme) by connecting the device to four syringe pumps (neMESYS Plugin) via polyethylene tubing (Intramedic Clay Adams Brand PE20) and plastic syringes. HFE 7500 and PFPE–Tris surfactant (2 wt%) were mixed and injected with a flow rate of 2000 µL $h^{-1}$. The precursor polymers 4-arm PEG-thiol 10 000 g $mol^{-1}$ (300 g $L^{-1}$) and linear PEG-acrylate 2000, 5000, or 7500 g $mol^{-1}$ (120, 300, or 450 g $L^{-1}$) were dissolved in phosphate buffer (DPBS) and then equally injected with a flow rate of 75 µL $h^{-1}$. Osteoblast cells (MG-63 GFP) were also injected in the middle channel with a flow rate of 75 µL $h^{-1}$. The cells were cultivated in petri dishes with an area of 11.9 $cm^2$ and were detached from the dishes for microfluidic experiments. For that purpose, cells were rinsed with phosphate buffer (DPBS), incubated with trypsin EDTA solution to release the cells, and then centrifuged for 5 min at 1000 rpm. The resulting cell pellet was resuspended in DMEM (1% Gl, 10% FBS, 1% P/S) and 15% OptiPrep (0.333 mL). In each experiment, four petri dishes were used with a cell population density of approximately 80%, which corresponded to $3.13 \times 10^7$ cells per microfluidic experiment. Cell counting was performed with a Neubauer counting chamber. The cell suspension was injected in the microfluidic devices, whereby the cell containing droplets were collected at 37 °C. Depending on the polymer system, microgels were then purified after 30–60 min with a 50% solution of 1*H*,1*H*,2*H*,2*H*-perfluoro-1-octanol in HFE7500 in several trituration steps and then transferred into DMEM (1% Gl, 10% FBS, 1% P/S). Cell-containing microgels are incubated over several weeks at 5% $CO_2$ and 37 °C and are analyzed by optical microscopy (Zeiss Axio) and 2D, as well as 3D confocal microscopy.

*Cell- and Vaterite-Containing Microgels*: Droplet templating was carried out with the PDMS device shown in Figure 1 (in the middle of the scheme) by connecting the device to five syringe pumps (neMESYS Plugin and Harvard pump) via polyethylene tubing (Intramedic Clay Adams Brand PE20) and plastic syringes. HFE 7500 and PFPE–Tris surfactant (2 wt%) were mixed and injected with a flow rate of 3000 µL $h^{-1}$. The precursor polymers 4-arm PEG-thiol 10 000 g $mol^{-1}$ (300 g $L^{-1}$) and linear PEG-acrylate 2000 g $mol^{-1}$ (120 g $L^{-1}$) were dissolved in phosphate buffer (DPBS) and then equally injected with a flow rate of 75 µL $h^{-1}$. Additionally, 3.4% w/v of vaterite particles in ethylene glycol were injected with a flow rate of 50 µL $h^{-1}$ to obtain a total vaterite concentration of 1.0% w/v in microgels, while osteoblast cells (MG-63 GFP) in DMEM were injected with a flow rate of 75 µL $h^{-1}$. The cells were cultivated in petri dishes with an area of 11.9 $cm^2$ and were detached from the dishes for microfluidic experiments. For that purpose, cells were rinsed with phosphate buffer (DPBS), incubated with trypsin EDTA solution to release the cells, and then centrifuged for 5 min at 1000 rpm. The resulting cell pellet was resuspended in DMEM (1% Gl, 10% FBS, 1% P/S) and 15% OptiPrep. In each experiment, four petri dishes were used with a cell population density of approximately 80%, which corresponded to $3.13 \times 10^7$ cells per microfluidic experiment. Cell counting was performed with a Neubauer counting chamber. After injection, the vaterite- and cell-containing droplets were collected at 37 °C and then purified after 30–60 min with a 50% solution of 1*H*,1*H*,2*H*,2*H*-perfluoro-1-octanol in HFE7500 in several trituration steps and then transferred into DMEM (1% Gl, 10% FBS, 1% P/S). Vaterite and cell-containing microgels were incubated over several weeks at 5% $CO_2$ and 37 °C and were analyzed by optical microscopy (Zeiss Axio) and 2D, as well as 3D confocal microscopy.

*Testing of Gels for the Presence of Endotoxin*: The rapid induction of E-selectin on endothelial cells in culture after exposure to endotoxin (LPS) was shown to be a very sensitive method to detect the presence of endotoxin in solutions at femtogram levels.[20,21] This method was used to examine gels made from the individual precursor molecules to show that they were free of endotoxin. Vaterite synthesis described in this publication was previously shown to be free of endotoxin.[10] Briefly, the individual precursors (4-arm PEG-thiol 10 000 g $mol^{-1}$ [160 g $L^{-1}$] and linear PEG-acrylate 5000 g $mol^{-1}$ [160 g $L^{-1}$] in phosphate buffer) were combined to form a gel in a microcentrifuge tube. After polymerization, 1 mL of DPBS was added to the tube and incubated for 24 h at 37 °C. After 24 h, the supernatant was removed from the gels and an aliquot (20 µL) was added to HUVEC cells growing in one well of an eight-well chamber slide. The gel remaining in the tube was removed via pipetting and placed onto HUVEC cells in a second well in the chamber slide with fresh media. Cells were also exposed to 1 µg $mL^{-1}$ of endotoxoin (LPS, Sigma) or left untreated (negative control) in additional wells. After 4 h, cells were washed 2× with PBS and fixed with paraformaldehyde and then stained with antibody against E-selectin (1:100 E-selectin, Monosan [M6010], Netherlands). After 1 h, cells were washed 4× with PBS and then the secondary antibody was added (1:1000, anti-mouse Alexa Fluor 488, Molecular Probes) and incubated at room temperature. After 1 h, cells were washed and Hoechst Dye 33342 (1:10000 in PBS, Molecular Probes) was added to stain the nuclei. After 5 min, cells were washed 2× with PBS, mounting medium was added (Fluoroshield, ImmunoBioScience Corp.), and cells were examined by fluorescence microscopy.

*Toxicity of Gels*: The viability of cells was measured by the addition of resazurin to cells in culture in the presence and absence of gels (4-arm PEG-thiol 10 000 g $mol^{-1}$ [300 g $L^{-1}$] and linear PEG-acrylate 5000 g $mol^{-1}$ [300 g $L^{-1}$] in phosphate buffer). Resazurin was used to measure the metabolic activity of living cells, which is converted by a redox reaction

to the fluorescent compound resorufin and this can be measured in a fluorescent ELISA reader. Gels were added to wells in a 96-well plate. After polymerization, 20 000 cells/96 well (MG-63) were added to the wells and incubated for 24 h and then 20 µL of resazurin stock solution (12 mg resazurin in 100 mL Hanks' Balanced Salt Solution with $Ca^{2+}$ and $Mg^{2+}$, Sigma-Aldrich) was added and incubated for a further 2 h at 37 °C. After this, 100 µL was removed from each well and placed into a new 96-well plate and examined in an ELISA reader (TECAN Spark 10M, 530–570 nm excitation and 580–100 nm emission). The amount of resorufin produced by cells exposed to gels was compared to unexposed cells set at 100%.

*Rheology Measurements*: To compare the gelation time and stiffness of the several polymer systems investigated in this study (10K/2K, 10K/5K, and 10K/7.5K), time-dependent rheology measurements were carried out using an Anton Paar modular compact rheometer of type MCR 302 (Anton Paar, Graz, Austria) equipped with a plate–plate measuring system PP08, with a radius of 8 mm and a plate–plate gap distance of 0.4 mm at 21 °C. For all measurements, a solvent trap was used to suppress evaporation of the solvent. The samples were prepared by mixing the precursor polymers (4arm PEG-thiol 10K [300 g $L^{-1}$] and linear PEG-acrylate 2K [120 g $L^{-1}$], 5K [300 g $L^{-1}$], or 7.5K [450 g $L^{-1}$]), dissolved in phosphate buffer, DMEM, or a mixture of both (ratio 6:1) prior to beginning the measurements. For this purpose, 18 µL of sample was applied. Experiments were carried out at a constant shear amplitude of 1% and a shearing frequency of 6.28 rad $s^{-1}$. Measurements in the linear-viscoelastic (LVE) regime were confirmed by amplitude sweeps, whereby the frequency remained constant at 6.28 rad $s^{-1}$ and the amplitude varied between 0.01% and 100% deformation. Also, frequency sweeps were done in a frequency range of 100–0.1 rad $s^{-1}$, at a fixed amplitude of 1% within the LVE regime of the sample.

*FCS*: Experiments were done with a Leica TCS-SP8 AOBS SMD microscope and a SymPhoTime 64 analysis software from PicoQuant. Measurements are performed with a HCPLAPO CS2 63x/1.20 water objective, an argon laser with 20% intensity, and an HyD SMD 1 detector. For sample preparation, gels (4-arm PEG-thiol 10 000 g $mol^{-1}$ [300 g $L^{-1}$] and linear PEG-acrylate 2000 g $mol^{-1}$ [120 g $L^{-1}$], 5000 g $mol^{-1}$ [300 g $L^{-1}$], and 7500 g $mol^{-1}$ [450 g $L^{-1}$] in phosphate buffer) were prepared in an eight-well plate (Ibidi). After gelation, gels were incubated in a dye solution at room temperature overnight. A 6 nM solution of sulforhodamine B was used, as well as a 6 nM solution of BSA-labeled with tetramethyl rhodamine (both prepared in DPBS). All measurements were carried out in the gel volume, whereby five points for each gel are selected. For fitting with SymPhoTime 64 analysis software, the 3D Gaussian triplet model was selected. Calibration was performed with a sulforhodamine B solution (6 nM) in phosphate buffer, with a diffusion coefficient of 440 $\mu m^2$ $s^{-1}$ (22 °C).[23]

*Swelling Measurements*: Droplet templating was carried out with the PDMS device shown in Figure 1 (on the left and right side of the scheme) by connecting the device to four syringe pumps (neMESYS Plugin) via polyethylene tubing (Intramedic Clay Adams Brand PE20) and plastic syringes. The precursor polymers 4-arm PEG-thiol 10 000 g $mol^{-1}$ (300 g $L^{-1}$) and linear PEG-acrylate 2000, 5000, or 7500 g $mol^{-1}$ (120, 300, or 450 g $L^{-1}$) were dissolved in phosphate buffer and then equally injected with a flow rate of 75 µL $h^{-1}$, while pure DPBS was injected in the middle channel with a flow rate of 25 µL $h^{-1}$. The microgels were then purified after 1 h with a 50% solution of 1*H*,1*H*,2*H*,2*H*-perfluoro-1-octanol in HFE7500 in several trituration steps and then transferred into DPBS or DMEM (1% Gl, 10% FBS, 1% P/S). Microgels were incubated in diverse DPBS solutions, which differed from each other in the pH value. Phosphate buffer (pH 5) was prepared by acidifying DPBS (pH 7.2) with HCl, while phosphate buffer of pH 9 was prepared by adding aqueous NaOH solution. The swelling behavior of microgels was then observed by optical microscopy (Zeiss Axio) and ImageJ was used to determine the size of the microgels. All measurements were done at room temperature. In addition, measurements were performed at physiological conditions. For this purpose, microgels were transferred into DMEM (1% Gl, 10% FBS, 1% P/S) and then incubated for several days at 5% $CO_2$ and 37 °C. The swelling behavior of the microgels was evaluated as described above.

*Statistical Analysis*: Quantitative data and sample size of cell viability results are given as mean ± standard deviation (SD) and numbers (*n*), respectively. Excel from Microsoft and Origin from OriginLab were the softwares used for statistical analysis.

## Supporting Information

Supporting Information is available from the Wiley Online Library or from the author.

## Acknowledgements

Parts of the results of this study were acquired with a confocal laser scanning microscope funded in part by the Major Research Instrumentation Program of the German Research Foundation under grant No. INST 247/878-1 FUGG. The authors wish to thank Andrea Schiffmann, Cornelia Seidel, Sandra Decker, Prof. Gerald Gimpl, and Dr. Thies Schröder (JGU Mainz) for initial support in cellular biology. Further thanks go to Dr. Ute Kolb and Dr. Hajo Frerichs (JGU Mainz) for SEM measurements. The authors also thank Prof. Andreas Stenglein (JGU Mainz) for the design of photomasks, as well as Max Männel and Dr. Julian Thiele (IPF Dresden) for their printing. The authors gratefully acknowledge the general support and assistance by Dr. Karl Fischer (JGU Mainz).

## Conflict of Interest

The authors declare no conflict of interest.

## Keywords

biotherapeutics, bone tissue engineering, microfluidics, microgels, vaterite

Received: December 18, 2019
Revised: April 8, 2020
Published online: May 6, 2020

[1] M. R. Iaquinta, E. Mazzoni, M. Manfrini, A. D'Agostino, L. Trevisiol, R. Nocini, L. Trombelli, G. Barbanti-Brodano, F. Martini, M. Tognon, *Int. J. Mol. Sci.* **2019**, *20*, 618.
[2] K. Zhang, S. Wang, C. Zhou, L. Cheng, X. Gao, X. Xie, J. Sun, H. Wang, M. D. Weir, M. A. Reynolds, N. Zhang, Y. Bai, H. H. K. Xu, *Bone Res.* **2018**, *6*, 31.
[3] Y. Zeng, J. Hoque, S. Varghese, *Acta Biomater.* **2019**, *93*, 152.
[4] J. Scheinpflug, M. Pfeiffenberger, A. Damerau, F. Schwarz, M. Textor, A. Lang, F. Schulze, *Genes* **2018**, *9*, 247.
[5] K. N. Tu, *P T Community* **2018**, *43*, 92.
[6] V. Paspaliaris, G. Kolios, *Stem Cells Int.* **2019**, *2019*, 1730978.
[7] M. Dang, L. Saunders, X. Niu, Y. Fan, P. X. Ma, *Bone Res.* **2018**, *6*, 25.
[8] a) X. Li, B. Cho, R. Martin, M. Seu, C. Zhang, Z. Zhou, J. S. Choi, X. Jiang, L. Chen, G. Walia, J. Yan, M. Callanan, H. Liu, K. Colbert, J. Morrissette-McAlmon, W. Grayson, S. Reddy, J. M. Sacks, H.-Q. Mao, *Sci. Transl. Med.* **2019**, *11*, 490; b) Y. Wu, L. Wang, B. Guo, P. X. Ma, *J. Mater. Chem. B* **2014**, *2*, 3674; c) R. Dong, X. Zhao, B. Guo, P. X Ma, *ACS Appl. Mater. Interfaces* **2016**, *8*, 17138; d) Guo, J. Qu, X. Zhao, M. Zhang, *Acta Biomater.* **2019**, *84*, 180; e) Y. Wu, L. Wang, B. Guo, P. X. Ma, *ACS Nano* **2017**, *11*, 5646.

[9] a) D. Shi, J. Shen, Z. Zhang, C. Shi, M. Chen, Y. Gu, Y. Liu, *J. Biomed. Mater. Res., Part B* **2019**, *107*, 2040; b) D. Anandan, S. M. Stella, N. A. Nambiraj, U. Vijayalakshmi, A. K. Jaiswal, *J. Biomed. Mater. Res., Part A* **2018**, *106*, 3267; c) S. Chen, Y. Shi, X. Zhang, J. Ma, *J. Biomed. Mater. Res.* **2019**, *107*, 2512; d) W. Zheng, X. Jiang, *Acc. Chem. Res.* **2018**, *51*, 3166.
[10] R. J. Havlik, *Plast. Reconstr. Surg.* **2002**, *110*, 1176.
[11] R. Schröder, H. Pohlit, T. Schüler, M. Panthöfer, R. E. Unger, H. Frey, W. Tremel, *J. Mater. Chem. B* **2015**, *3*, 7079.
[12] R. Schröder, L. Besch, H. Pohlit, M. Panthöfer, W. Roth, H. Frey, W. Tremel, R. E. Unger, *J. Tissue Eng. Regener. Med.* **2018**, *12*, 1754.
[13] T. E. L. Douglas, A. Łapa, K. Reczyńska, M. Krok-Borkowicz, K. Pietryga, S. K. Samal, H. Declercq, D. Schaubroeck, M. Boone, P. Van Der Voort, K. De Schamphelaere, C. V. Stevens, V. Bliznuk, L. Balcaen., B. V. Parakhonskiy, F. Vanhaecke, V. Cnudde, E. Pamuła, A. G. Skirtach, *Biomed. Mater.* **2016**, *11*, 065011.
[14] E. Kapourani, F. Neumann, K. Achazi, J. Dernedde, R. Haag, *Macromol. Biosci.* **2018**, *18*, 1800116.
[15] a) B. V. Slaughter, S. S. Khurshid, O. Z. Fisher, A. Khademhosseini, N. A. Peppas, *Adv. Mater.* **2009**, *21*, 3307; b) R. Langer, J. P. Vacanti, *Science* **1993**, *260*, 920; c) Y. Lu, W. Zhang, J. Wang, G. Yang, S. Yin, T. Tang, C. Yu, X. Jiang, *Int. J. Oral Sci.* **2019**, *11*, 17.
[16] S. Seiffert, *ChemPhysChem* **2013**, *14*, 295.
[17] P. de Vos, H. A. Lazarjani, D. Poncelet, M. M. Faas, *Adv. Drug Delivery Rev.* **2014**, *67-68*, 15.
[18] a) T. Rossow, J. A. Heyman, A. J. Ehrlicher, A. Langhoff, D. A. Weitz, R. Haag, S. Seiffert, *J. Am. Chem. Soc.* **2012**, *134*, 4983; b) S. Hackelbusch, T. Rossow, D. Steinhilber, D. A. Weitz, S. Seiffert, *Adv. Healthcare Mater.* **2015**, *4*, 1841; c) D. Steinhilber, T. Rossow, S. Wedepohl, F. Paulus, S. Seiffert, R. Haag, *Angew. Chem., Int. Ed.* **2013**, *52*, 13538.
[19] T. Schüler, W. Tremel, *Chem. Commun.* **2011**, *47*, 5208.
[20] R. E. Unger, *Adv. Biomater. Devices Med.* **2014**, *1*, 38.
[21] R. E. Unger, K. Peters, A. Sartoris, C. Freese, C. J. Kirkpatrick, *Biomaterials* **2014**, *35*, 3180.
[22] S. Hackelbusch, T. Rossow, H. Becker, S. Seiffert, *Macromolecules* **2014**, *47*, 4028.
[23] P.-O. Gendron, F. Avaltroni, K. J. Wilkinson, *J. Fluoresc.* **2008**, *18*, 1093.
[24] J. Wu, C. Zhao, W. Lin, R. Hu, Q. Wang, H. Chen, L. Li, S. Chen, J. Zheng, *J. Mater. Chem. B* **2014**, *2*, 2983.
[25] a) T. Kraehenbuehl, P. Zammaretti, A. J. Van der Vlies, R. G. Schoenmakers, M. P. Lutolf, M. E. Jaconi, J. A. Hubbell, *Biomaterials* **2008**, *29*, 2757; b) D. Loessner, K. S. Stok, M. P. Lutholf, D. W. Hiutmacher, J. A. Clements, S. C. Rizzi, *Biomaterials* **2010**, *31*, 8494.
[26] E. E. Hui, S. N. Bhatia, *Proc. Natl. Acad. Sci. USA* **2007**, *104*, 5722.
[27] Y.-L. Chiu, H. F. Chan, K. K. L. Phua, Y. Zhang, S. Juul, B. R. Knudsen, Y.-P. Ho, K. W. Leong, *ACS Nano* **2014**, *8*, 3913.